Spring 2024

Generation, Dynamics, and Interaction of Quartic Solitary Waves in Nonlinear Laser Systems

Sabrina Hetzel
Southern Methodist University, shetzel@smu.edu

GENERATION, DYNAMICS, AND INTERACTION
OF QUARTIC SOLITARY WAVES
IN NONLINEAR LASER SYSTEMS

Approved by:

Dr. Alejandro Aceves
Professor

Dr. Andrea Barreiro
Associate Professor, Graduate Advisor

Dr. Benno Rumpf
Associate Professor

Dr. Ross Parker
Research Scientist

GENERATION, DYNAMICS, AND INTERACTION OF QUARTIC SOLITARY WAVES IN NONLINEAR LASER SYSTEMS

A Dissertation Presented to the Graduate Faculty of the

Dedman College

Southern Methodist University

in

Partial Fulfillment of the Requirements

for the degree of

Doctor of Philosophy

with a

Major in Applied and Computational Mathematics

by

Sabrina Hetzel

B.S., Economics, Tarleton State University
B.S., Mathematics, Tarleton State University
M.S., Applied and Computational Mathematics, Southern Methodist University

May 11, 2024

Acknowledgments

I would like to acknowledge my advisor, Dr. Alejandro Aceves, whose kindness, wisdom, and direction greatly influenced the type of researcher and mentor I have become. Thank you for everything.

I would like to acknowledge Dr. Ross Parker, who had a significant impact on me as a second mentor in my research. Thank you for all your help and answering any and all questions I had.

I would like to thank my other committee members, Dr. Andrea Barriero and Dr. Benno Rumpf, for their recommendations and instruction.

I would like to thank Dr. Andrea Blanco-Redondo for the incredibly valuable exchanges we have had over the years that have influenced the directions taken in this research to ensure the work done is beneficial and relevant to experimentalists working in labs.

I would like to acknowledge the generous support from the National Science Foundation (NSF) Research Training Group (RTG) grant, Southern Methodist University's Moody School of Graduate and Advanced Studies for the Dean's Dissertation Fellowship, and the Department of Mathematics at Southern Methodist University for the Haberman Dissertation Fellowship funding sources that made this possible.

I would like to thank my friends, Molly Robinson and Elyssa Sliheet, who were with me since the beginning of graduate school. They were the best possible people to have together in my cohort and made taking classes, studying, and doing research more enjoyable and manageable knowing we had each other's backs.

I would like to thank my family for their continued support throughout the years. Thank you for your continued encouragement and excitement during this time in my life.

Lastly, I would like to thank my partner, Preston Ward. Thank you for your love, confidence in me, and persistence. I definitely would not have gotten this far without you.

Hetzel, Sabrina

B.S., Economics, Tarleton State University
B.S., Mathematics, Tarleton State University
M.S., Applied and Computational Mathematics, Southern Methodist University

Generation, Dynamics, and Interaction of Quartic Solitary Waves in Nonlinear Laser Systems

Advisor: Dr. Alejandro Aceves

Doctor of Philosophy degree conferred May 11, 2024

Dissertation completed May 1, 2024

Solitons are self-reinforcing localized wave packets that have remarkable stability features that arise from the balanced competition of nonlinear and dispersive effects in the medium. Traditionally, the dominant order of dispersion has been the lowest (second), however in recent years, experimental and theoretical research has shown that high, even order dispersion may lead to novel applications. Here, the focus is on investigating the interplay of dominant quartic (fourth-order) dispersion and the self-phase modulation due to the nonlinear Kerr effect in laser systems. One big factor to consider for experimentalists working in laser systems is the effect of noise on the inputs to these systems. Therefore, I numerically analyze the generation of localized states arising from dominant quartic dispersion where noise is added on the inputs to the laser system and the resulting robustness of these states. In addition, I also examine the interaction of solitary waves with dominant quartic dispersion in different media and how these results can differ from the conventional case of dominant quadratic dispersion. The results show that the behavior that is exhibited for the quadratic case for generation of pulses is maintained and furthermore, there are increased opportunities for stable localized states in quartic Kerr media.

TABLE OF CONTENTS

LIST OF FIGURES

LIST OF TABLES

This is dedicated to my mom who inspired me to love numbers and to my dad who understands my passion for fireflies.

Chapter 1

Introduction and Background

The concept of solitons, solitary waves that propagate without dispersing or dissipating, has intrigued scientists and engineers since their first observation in the 19th century. In 1834, Scottish engineer John Scott Russell made a groundbreaking observation of a solitary wave traveling along a canal, which sparked scientific interest in solitary wave phenomena [34]. Russell's subsequent investigations laid the groundwork for the study of solitons, culminating in his publication of "Report on Waves" in 1844. Building upon Russell's empirical observations, Dutch physicists Diederik Korteweg and Gustav de Vries formulated the Korteweg-de Vries (KdV) equation in the late 19th century, providing a mathematical framework for describing soliton behavior in shallow water waves [22]. The KdV equation, a nonlinear partial differential equation, exhibited soliton solutions that preserved their shape and velocity over time, thus elucidating the underlying dynamics of solitons in certain physical systems.

Throughout the 20th century, advancements in nonlinear science further expanded our understanding of solitons and their manifestations in diverse physical phenomena. In the realm of optics, the discovery of soliton-like behavior in optical fibers revolutionized telecommunications in the 1970s [18]. Optical solitons, governed by the nonlinear Schrodinger equation, enabled the transmission of information over long distances without distortion or dispersion, laying the foundation for modern fiber-optic communication networks. The practical implementation of optical solitons highlighted the profound technological implications of soliton physics in real-world applications.

Theoretical developments in integrable systems provided a deeper understanding of solitons as solutions to nonlinear differential equations possessing an infinite number of conserved

quantities [41]. Solitons emerged as fundamental objects in integrable systems, exhibiting remarkable properties such as stability and non-dispersiveness. The mathematical structure of integrable systems shed light on the underlying mechanisms governing soliton dynamics, facilitating the exploration of soliton interactions, collisions, and other phenomena.

Current research efforts continue to explore new frontiers in soliton physics, encompassing interdisciplinary investigations across fields such as condensed matter physics, biophysics, and quantum computing. Solitons hold promise for applications in emerging technologies, including quantum information processing and nonlinear optics [2]. By leveraging their unique properties, researchers aim to develop novel approaches for information encoding, transmission, and manipulation. Moreover, the exploration of fascinating phenomena in topological materials and other complex systems opens avenues for further theoretical and experimental investigations.

The history of solitons embodies the interdisciplinary nature of scientific inquiry, spanning centuries of empirical observations, theoretical developments, and technological breakthroughs. From their humble origins in 19th-century canal observations to their pervasive presence in modern telecommunications and beyond, solitons have left a significant mark on our understanding of nonlinear wave phenomena. As researchers continue to unravel the mysteries of solitons and harness their potential in cutting-edge technologies, their journey remains an ongoing saga of discovery and innovation.

A soliton is a stable, localized wave packet that retains its shape while moving at a constant velocity during propagation through a medium. They also recover after collision with other solitons with no loss or change to their shape [21]. Their formation is possible through the balanced competition of dispersion and nonlinearity. This will be discussed in more detail in section 1.1. Briefly though, the order of dispersion effects the spreading of the wave. Since their first realization in optics, solitons in lasers were formed balancing negative second order dispersion and Kerr nonlinearity. Historically, higher-order dispersion was

seen as a detrimental factor that limited the pulse duration achievable [9] or led to soliton instabilities and energy loss [20]. This thinking changed in 2016 when it was experimentally demonstrated using dominant negative fourth order dispersion in a nonlinear Kerr medium, one could obtain what was named "pure quartic solitons" [5]. Using a dispersion engineered photonic crystal waveguide, the group was able to design a laser system that had small positive second order dispersion, virtually zero third order dispersion, and strong negative fourth order dispersion. They thus modeled it using a modified nonlinear schrodinger equation with fourth order dispersion (discussed in section 1.2).

Since their realization, there have been others that have worked in the experimental and theoretical analysis of other sorts of optical systems that could generate pure quartic solitons. These include microresonators which are small-scale optical devices that confine light within a small physical volume. There are other effects that must be taken into consideration when dealing with ultra-short pulses, namely the Raman effect which is non-negligible for this case [25]. Here, we do not consider the Raman effect as it adds another layer of complexity to the analysis carried out in this report. However, it would be something to consider and expand upon in the future when regarding these higher-order dispersion engineered solitons for short-pulse durations.

1.1. Dispersion and Nonlinearity

Solitons arise from the balanced competition of dispersion and the nonlinear effect of the medium, called the Kerr effect. Dispersion refers to the phenomena where different wavelengths of light travel at different speeds through a medium, causing the light to spread out or disperse over time. It is a crucial consideration in the design and operation of optical systems, particularly in applications such as telecommunications, spectroscopy, and optical imaging. Various techniques, such as dispersion compensation and dispersion engineering, are employed to mitigate the effects of dispersion and optimize the performance of optical devices and systems. Understanding and controlling dispersion is essential for achieving

high-quality and reliable optical communication and imaging. There are different types of dispersion encountered in optics, namely:

1. **Chromatic dispersion** refers to the dispersion of light over a range of wavelengths, leading to the separation of colors or spectral components. This type of dispersion can cause pulses of light to spread out in time, limiting the ability to transmit information over long distances without distortion. Chromatic dispersion is particularly significant in optical communication systems, where it can degrade signal quality and limit transmission distances.

2. **Material dispersion** occurs due to the frequency-dependent refractive index of a material. Different materials exhibit different levels of dispersion, with some materials dispersing light more than others. In general, materials with a higher refractive index tend to have stronger dispersion effects. This dispersion is a fundamental property of optical materials and can significantly affect the performance of optical systems and lead to interesting applications such as novel lasers.

3. **Modal dispersion** occurs in optical waveguides, such as optical fibers, where the structure of the waveguide causes different wavelengths of light to propagate at different speeds. This dispersion arises from the waveguide's geometry and can be influenced by factors such as core size, refractive index profile, and wavelength of operation. Modal dispersion can limit the bandwidth and data transmission rates of optical communication systems.

4. **Polarization mode dispersion (PMD)** occurs when light waves with different polarizations travel through an optical medium at different speeds. PMD can result from birefringence in optical fibers or other polarization-dependent effects. PMD can lead to distortion and broadening of optical pulses, affecting the performance of high-speed

communication systems. For the work presented in this paper, we do not consider the effects of PMD.

Consider light propagating in a guided-wave structure with a core refractive index, n_{core}, surrounded by a cladding refractive index, $n_{cladding}$ and propagation constant β [12]. The effective refractive index seen by the field in general is n_{eff} and lies between $n_{cladding} \leq n_{eff} \leq n_{core}$. Dispersion describes how n_{eff} of a medium depends on wavelength. For short wavelengths (high frequency), the light is almost entirely confined to the core so that $n_{eff} \approx n_{core}$. For long wavelengths (low frequency), the light is poorly confined and close to modal cutoff so that $n_{eff} \approx n_{cladding}$. When light propagates in a waveguide, it experiences dominant waveguide dispersion even over material dispersion. The total dispersion is approximately the sum of all the different types of dispersion. For frequency ω, in general, $\beta = \beta(\omega)$ but we could consider a limited width on the frequency spectrum. In this case, we only require $\beta(\omega)$ over a relatively narrow bandwidth centered at ω_0 and using Taylor series around ω_0,

$$\beta(\omega) - \beta(\omega_0) = \beta_1\Omega + \frac{\beta_2}{2!}\Omega^2 + \frac{\beta_3}{3!}\Omega^3 + ... \tag{1.1}$$

where $\Omega = \omega - \omega_0$ and $\beta_m = \frac{\partial^m \beta}{\partial \omega^m}(\omega = \omega_0)$ is the m-th dispersion order coefficient. Dispersion has an important relation to the group velocity, v_g, of the light, namely

$$\frac{1}{v_g} = \frac{\partial \beta}{\partial \omega}(\omega = \omega_0) \tag{1.2}$$

Hence, β_2 provides the lowest order description of dispersion and so its effect would be expected to dominate over higher-order terms. However with proper engineering design, one can shift the leading order term to fourth.

Nonlinearity in optics refers to the property that the index of refraction depends on the intensity itself. Nonlinear optical effects arise when the intensity of light becomes sufficiently

high to induce changes in the optical properties of the medium. It was only with the invention of lasers that pulses had high intensity. By varying the intensity or wavelength of the input light, nonlinear materials can produce different colors in the output. This is particularly useful in applications such as frequency doubling for laser sources or in nonlinear frequency conversion processes for generating new colors. Nonlinear optics plays a crucial role in various applications, including telecommunications, laser technology, imaging, and quantum optics. There are many types of nonlinear optical effects, but here we focus only on the Kerr effect. The Kerr effect is a nonlinear optical phenomenon in which the refractive index of a material changes in response to the intensity of light passing through it. This change in refractive index is instantaneous and proportional to the square of the light's intensity. The Kerr effect is responsible for phenomena such as self-focusing, self-phase modulation, and cross-phase modulation, which can occur in optical fibers, photonic devices, and nonlinear crystals.

In optics, self-focusing refers to nonlinear optical process where a beam of light concentrates or focuses upon itself as it propagates through the medium [10]. It was first predicted by Gurgen Askaryan [3] in the early 1960s and experimentally observed a few years later by studying the interaction of ruby lasers with gasses and liquids [23]. This effect arises due to the interaction between the electromagnetic field of the light and the medium's refractive index, which can be modified by the intensity of the light itself. The change in refractive index caused by the Kerr effect leads to a focusing effect on the beam. This focusing occurs because regions of higher intensity experience a greater change in refractive index, causing the light to bend towards regions of lower refractive index [7]. This results in the beam of light becoming more tightly focused as it propagates through the medium. As light propagates through the nonlinear medium, its intensity can become high enough to induce self-phase modulation (SPM). This means that the phase of the light wave changes nonlinearly with its intensity. SPM is an important effect in laser systems that use short, intense pulses of light [38].

Self-defocusing is the counterpart to self-focusing in optics. While self-focusing refers to the phenomenon where a beam of light concentrates or focuses upon itself as it propagates through a nonlinear medium, self-defocusing occurs when the beam spreads out as it travels through the medium. The process of formation is related to that of self-focusing, however, in this case, the nonlinear response of the medium leads to a decrease in refractive index in regions of higher intensity [7]. This causes the light beam to experience outward spreading rather than inward focusing.

1.2. Nonlinear Schrodinger Equation (NLSE)

The nonlinear Schrödinger equation (NLSE) is a universal partial differential equation very relevant in nonlinear optics. It describes the propagation of optical waves in nonlinear media, where the response of the medium depends nonlinearly on the intensity of the waves. The NLSE arises from the Schrödinger equation, which governs the behavior of quantum particles, by including additional nonlinear terms to account for interactions between waves. The generalized NLSE of the electric field envelope E is

$$-i\frac{\partial E}{\partial t} = -\frac{\beta_2}{2!}\frac{\partial^2 E}{\partial z^2} - i\frac{\beta_3}{3!}\frac{\partial^3 E}{\partial z^3} + \frac{\beta_4}{4!}\frac{\partial^4 E}{\partial z^4} + \gamma|E|^2 E$$

where we truncate the Taylor expansion of the dispersion part after the quartic term. Commonly, the Taylor expansion is truncated after the quadratic term and the NLSE results, which is integrable.

The term pure quartic solitons (PQS) was coined in [5] where the original experimental realization was seen exclusively arising from the interaction of negative quartic dispersion and Kerr nonlinearity. That is, considering when $\beta_2 = \beta_3 = 0$, PQSs are stationary solutions of the following quartic NLSE:

$$i\frac{\partial E}{\partial t} = \frac{\beta_4}{4!}\frac{\partial^4 E}{\partial z^4} - \gamma|E|^2 E \tag{1.3}$$

Similar to the standard nonlinear Schrodinger equation with only second-order dispersion, there are some conserved quantities of the quartic NLSE. Namely, the hamiltonian

$$\mathcal{H} = \int_{\mathbb{R}} \left(-\frac{\beta_4}{4!} \left| \frac{\partial^2 E}{\partial z^2} \right|^2 + \frac{\gamma}{2} |E|^4 \right) dz$$

is conserved, i.e. $\frac{d\mathcal{H}}{dz} = 0$. The NLSE is propagating freely with no losses or gains unlike the Lugiato-Lefever equation, which will be discussed in the next section and is the model considered in this paper, and is not conservative. The NLSE typically describes the propagation of an optical wave in a nonlinear medium that has applications in a wide range of fields such as fiber optic communication systems and ultrafast optics.

There are a couple main differences between PQS and conventional solitons, that is solitons with only second-order dispersion in the NLSE. As it relates to pulses, there are oscillations in the PQS tails which occur at low intensities. This unique characteristic is used in quantifying the interaction of pulses. Also, PQSs are non-integrable. The energy-width scaling laws are significantly different for short pulses with different orders of dispersion. The energy scales with the inverse pulse duration for conventional solitons and for PQSs, the energy scales with the cubic inverse pulse duration. Theoretical and experimental studies have shown that PQSs have an advantageous energy scaling, granting them the potential to achieve significantly higher energy than conventional solitons for short pulse durations. This leads to the potential for the generation of high-energy ultrashort optical pulses arising from the interplay of self-phase modulation and higher-order cavity dispersion. These two differences are indicated in figure 1.1.

1.3. Lugiato-Lefever Equation (LLE)

The Lugiato-Lefever equation (LLE) is a mean field approximation that models the propagation of pulses inside a cavity. It was first described in 1987 for phenomena leading to pattern formation in nonlinear optical systems [26]. The physics of a system described by

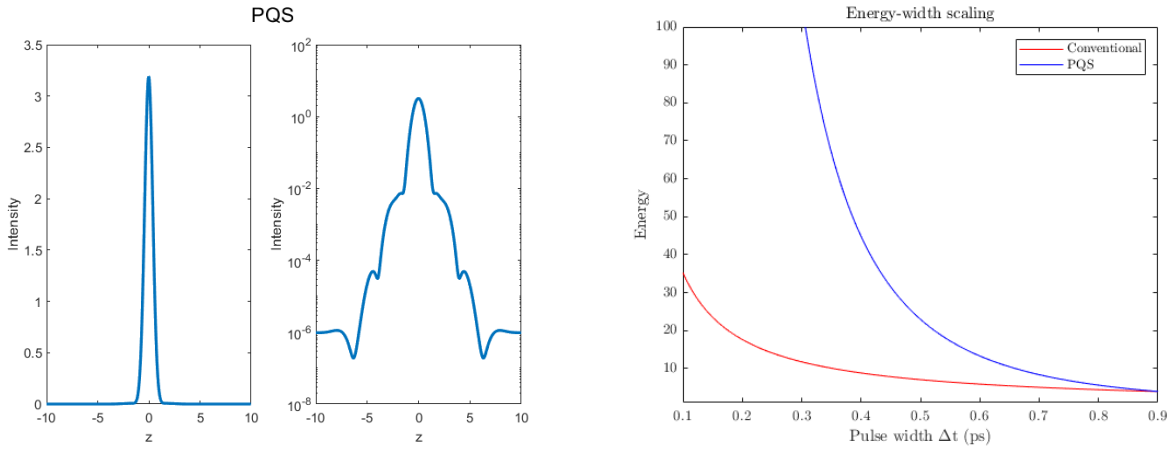

Figure 1.1: PQS properties

the LLE revolves around the dynamics of light inside an optical cavity. There are several key components with physical significance involved for light propagating in a cavity. The optical cavity itself could be a laser, microresonator, or others. The cavity confines light, allowing it to resonate and interact with itself. Inside the cavity, there are different optical elements such as crystals, fibers, mirrors, and grating to engineer dispersion. There are also nonlinear effects, meaning the optical properties of the medium change with the intensity of light. There could also be a difference between the frequency of the driving field and the resonant frequency of the cavity. This minimum difference between the two frequencies is what is known as detuning. When the driving frequency matches the cavity resonance, the system operates at its most efficient point. The light waves bounces between mirrors in the cavity which are not perfectly reflective, as we need some light to come out of the system to see the output. In fact, there are losses and gains in the system. There are linear losses, such as mirrors, absorption or scattering of light, and there are nonlinear losses due to effects like two-photon absorption. There is gain inserted into the system to offset these losses, such as an external laser source providing input light.

Figure 1.2 illustrates with a cartoon model for the propagation of light in a cavity. A light beam is inputted into the system where it bounces back and forth between the two mirrors. Since the mirrors aren't perfectly reflective, there is some loss introduced in the

system that is offset from the gain put in by the pump power. As stated above, Inside of the cavity, there are optical elements for engineering dispersion and nonlinearity. The left mirror is almost perfectly reflective whereas the right mirror is typically ninety percent reflective. The light that escapes the right mirror is the output measured for the system.

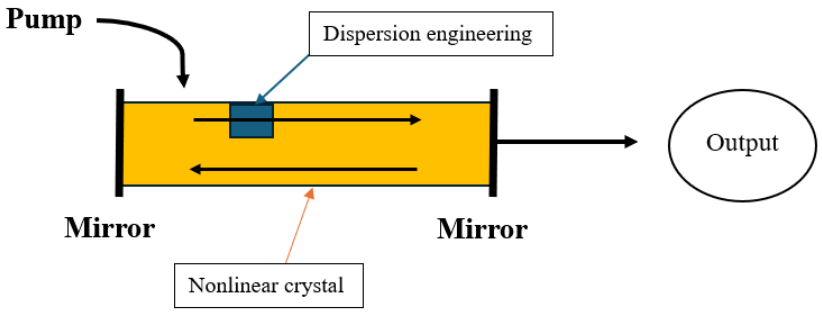

Figure 1.2: Diagram of physical model for LLE

Consider the modified Lugiato-Lefever equation with only fourth-order dipsersion for the electric field envelope E:

$$\frac{\partial E}{\partial t} = -(1 + i\theta)E + i\gamma|E|^2E + i\beta_4\frac{\partial^4 E}{\partial z^4} + P \tag{1.4}$$

The first term on the right-hand side describes cavity losses, θ is a cavity detuning parameter, and P is the pump power assumed to be constant. There has been some work at the consideration of a variable pump power, where P=P(z) ([8], [28]). For simplicity, we assume that P is constant. The nonlinearity coefficient is taken to be one and β_4 is the fourth-order dispersion parameter coefficient. The cubic nonlinearity here represents the nonlinear Kerr effect with γ being the nonlinerity coefficient. If $\gamma = 1$, this corresponds to the self-focusing case and if $\gamma = -1$, this corresponds to the self-defocusing case. The variable t is the time scale used for describing the evolution of the field envelope E over many cavity round trips and the variable z is the space coordinate describing the envelope's profile over a single cavity round trip. Negative fourth-order dispersion, $\beta_4 < 0$, can lead to stable bright pulses and

multi-pulse solutions. When there is positive fourth-order dispersion, $\beta_4 > 0$, this can lead to stable dark pulses and bright pulses.

In summary, solitons stand as remarkable structures emerging from the balance between dispersion and nonlinearity. Their unique properties, such as maintaining shape and velocity over long distances, make them pivotal in various applications. Understanding the dynamics of solitons can be facilitated by mathematical frameworks like the Nonlinear Schrodinger Equation (NLSE) and the Lugiato-Lefever Equation (LLE). The NLSE provides a broad description of nonlinear wave propagation, offering insights into soliton formation. Meanwhile, the LLE focuses on the specific dynamics of solitary waves within an optical cavity. Looking at the effects of fourth-order dispersion in these systems will help guide research in fields ranging from fiber optic communications to ultrafast optics and microresonator-based devices. Higher-order dispersion can potentially enhance the performance or capabilities of these systems, particularly in terms of having short-duration pulses with higher energy compared to those of dominant second-order dispersion with the same pulse-width.

Chapter 2

Existence and Stability of Continuous Wave Solutions of the Quartic LLE

This chapter relates to the existence and stability of continuous wave (CW) solutions of the quartic LLE. The existence of CW solutions of the LLE is well known [26], [16]. In the case of quadratic dispersion, linear stability analysis was further investigated in [36]. It has only been recently [33] that the stability of CW solutions has been investigated where dispersion in the LLE has been fourth order.

Unlike the quartic NLSE, the quartic LLE is non-conservative and exhibits a non-zero background state. In their original paper [26], Lugiato and Lefever demonstrate the existence of complex constant solutions to the LLE (with quadratic dispersion) with the well know cubic equation of dispersive optical bistability [15]. These known solutions of the LLE, in which we set all derivatives to zero, are known as continuous wave (CW) solutions. Clearly, their existence is independent of the order of dispersion. The CW solutions provide a baseline for understanding the behavior of the system and thus allowing us to gain insights into the fundamental properties. They also serve as starting points for stability analysis in order to determine whether they represent stable or unstable states of the system. However, the stability properties do depend on the order of dispersion. The existence and stability of CW solutions depend on the parameters of the LLE, such as the nonlinerity coefficient and detuning and pump power.

The continuous wave (CW) solutions, denoted E_s of equation (1.4) are found by setting all derivatives to zero, that is $\frac{\partial E}{\partial t} = \frac{\partial^4 E}{\partial z^4} = 0$. This leads to an algebraic equation dependent

on the parameters θ and P^2 (set $\gamma = 1$) that can be solved to find the CW solutions.

$$P^2 = |E_s|^2[1 + (\theta - |E_s|^2)^2]$$

Letting $I_s = |E_s|^2$, we have

$$I_s[1 + (\theta - I_s)^2] = P^2$$

which is the cubic equation of dispersive optical bistability, namely

$$I_s^3 - 2\theta I_s^2 + (\theta^2 + 1)I_s = P^2 \tag{2.1}$$

As it has been shown in previous work [26], this curve, shown in figure 2.1, is in the shape of an "S" and is thus typically referred to as the "S-curve". This curve exhibits what is called hysteresis behavior. Hysteresis refers to the dependence of a system's output not only on its current input, but also, on its history of past inputs. This is due to the response of the optical materials to external stimuli. Hysteris drives phenomena like optical instability that produces bifurcations that can lead to chaos.

You can fix θ or P, here the choice is to fix θ and vary the pump power P. This is traditionally what is done to analyze the stability of the CW solutions [26]. To show the existence of two CW solutions analytically, look at the points where the derivative $\frac{\partial P^2}{\partial I_s}$ is equal to zero:

$$\frac{\partial P^2}{\partial I_s} = \frac{\partial}{\partial I_s}[I_s^3 - 2\theta I_s^2 + (\theta^2 + 1)I_s] = 0 \tag{2.2}$$

$$3I_s^2 - 4\theta I_s + (\theta^2 + 1) = 0 \tag{2.3}$$

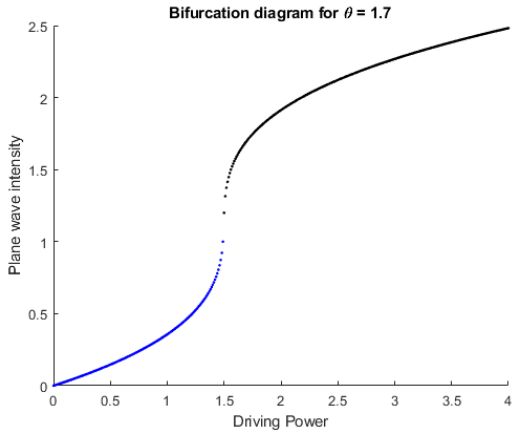

(a) Case where $\theta < \sqrt{3}$

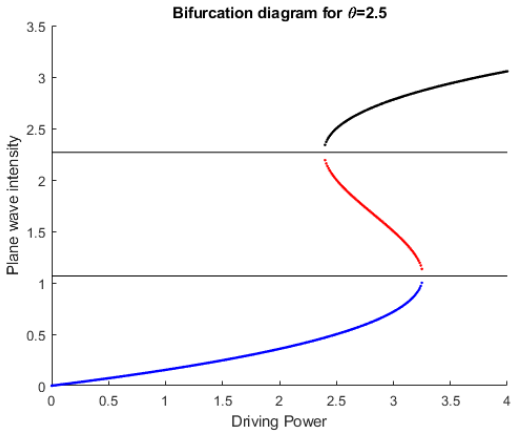

(b) Case where $\theta > \sqrt{3}$

Figure 2.1: Bifurcation plots of steady state plane wave solutions where the driving power (P^2) is plotted against intensity levels (I_s) showing a saddle-node bifurcation. (a) Blue line is when it is stable, black line is unstable. (b) Blue line is when it is stable, red line is when it is unstable, and black line is the modulation instability (MI). The horizontal lines are the values of $I_s^{1,2}$ from equation (2.4).

The solutions to equation (2.3) give the turning points of the bistable response, also known as the saddle-node bifurcations of the CW solutions [32]:

$$I_s^{1,2} = \frac{2\theta}{3} \pm \frac{1}{3}\sqrt{\theta^2 - 3} \tag{2.4}$$

Thus, the point when $\theta^2 = 3$, is a critical point. Whenever $\theta < \sqrt{3}$, there are no turning points and the system is monostable. This implies that for this case, I_s in equation (2.1) has one real root. When $\theta > \sqrt{3}$, there are two turning points and the system is bistable (see figure 2.1). This implies that for this case, I_s in equation (2.1) has three real roots.

In summary, the CW states are given by the cubic equation of dispersive optical bistability whose roots are determined by the value of the detuning parameter and the pump power. The CW solutions are equivalent for the LLE with second or fourth order dispersion but nevertheless, provide a baseline for further investigations into coherent structures due to bifurcations off of the S-curve shown in figure 2.1.

2.1. Linear Stability Analysis of Quartic LLE

This section presents the linear stability analysis of the CW solutions of the quartic LLE. The results are different than the second-order case presented in [36] and are given for both the self-focusing case and the self-defocusing case. By introducing an ansatz, we can analyze the regions of stability for the solutions given different parameter values. Introduce a transformation [36] into equation (1.4), namely, $E = E_s(1+A)$. This will yield the following equation:

$$\partial_t A = -(1+i\theta)A + i\beta_4\partial_z^4 A + i\gamma|E_s|^2(2A + A^* + 2|A|^2 + A^2 + |A|^2 A) \tag{2.5}$$

Equation (2.5) is fully equivalent to equation (1.4). The stability of the CW solutions can be analyzed by assuming A is small and linearizing equation (2.5) with respect to A. This must be considered with its complex conjugate, A^*, in which A is coupled with. Thus the linearized system reads

$$\frac{d}{dt}\begin{pmatrix} A \\ \\ A^* \end{pmatrix} = L \begin{pmatrix} A \\ \\ A^* \end{pmatrix}$$

where

$$L = \begin{pmatrix} -(1+i\theta) + i\beta_4\partial_z^4 + 2i\gamma|E_s|^2 & i\gamma|E_s|^2 \\ \\ -i\gamma|E_s|^2 & -(1-i\theta) - i\beta_4\partial_z^4 - 2i\gamma|E_s|^2 \end{pmatrix}$$

By introducing an ansatz that the perturbation A has the form of a plane-wave modulation, that is $exp(ikz + \sigma t)$, one can then obtain the characteristic eigenvalue equation:

$$\sigma^2 + 2\sigma + \zeta(|E_s|^2, \beta_4 k^4) = 0 \tag{2.6}$$

where

$$\begin{aligned}\zeta(|E_s|^2, \beta_4 k^4) &= (-(1+i\theta) + 2i\gamma|E_s|^2 + i\beta_4 k^4)(-(1-i\theta) - 2i\gamma|E_s|^2 - i\beta_4 k^4) - |E_s|^4 \\ &= (\beta_4 k^4)^2 - 2(\theta - 2\gamma|E_s|^2)(\beta_4 k^4) + ((1+\theta^2) - 4\gamma|E_s|^2\theta + 3\gamma^2|E_s|^4)\end{aligned}$$

The stationary solution is unstable when one of the roots of equation (2.6) has a positive real part for at least one choice of k. This amounts to the condition that the constant term ζ be negative [26]. The roots of $\zeta(|E_s|^2, \beta_4 k^4)$,

$$(\beta_4 k^4) = (\theta - 2\gamma|E_s|^2) \pm (\gamma^2|E_s|^4 - 1)^{1/2}$$

So, the interval of instability is

$$a^-(|E_s|^2) < \beta_4 k^4 < a^+(|E_s|^2)$$

where $a^{\pm}(|E_s|^2) = (\theta - 2\gamma|E_s|^2) \pm (|E_s|^4 - 1)^{1/2}$ with $\theta - 2\gamma|E_s|^2 > 0$ and $|E_s|^4 \geq 1$. Note that since γ is unitary, then $\gamma^2 = 1$.

There are two cases to consider, when $\gamma > 0$, self-focusing, and when $\gamma < 0$, self-defocusing. For the case of self-focusing, figure 2.2a shows the unstable domain for the self-focusing case when $\theta = 2$, $\theta = 5$. The red dot represents the minimum point which corresponds to the turning point for the onset of the instability [36]. It has coordinates

$$\beta_4 k_c^4 = \theta - 2, |E_s|_c^2 = 1$$

where $\theta > 2$ has physical meaning. For the case of self-defocusing, figure 2.2b shows the unstable domain for $\gamma = -1$ and $\theta = 1$, $\theta = 3$. The turning points of the instability have coordinates

$$\beta_4 k_c^4 = 2 + \theta, |E_s|_c^2 = 1$$

where $\theta > 0$ has physical meaning. As shown in the figures, as you increase θ, the curves shift along the horizontal line $|E_s|^2 = 1$.

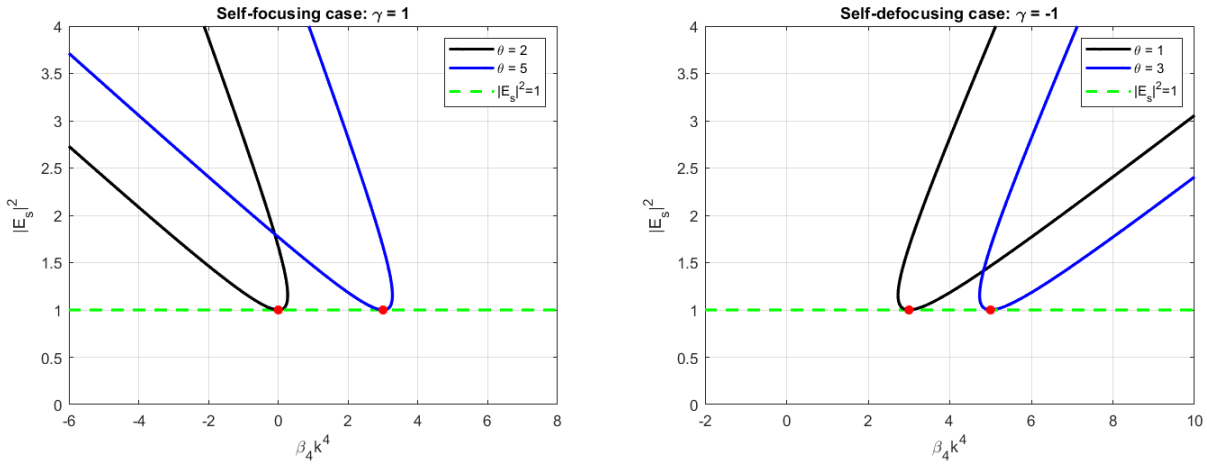

(a) Self-focusing case (b) Self-defocusing case

Figure 2.2: The figure shows the domain of the plane $(\beta_4 k^4, |E_s|^2)$ in which the CW solution is unstable for different values of θ.

In conclusion, the study of continuous wave (CW) states and their linear stability analysis offers valuable insights into the dynamics of nonlinear optical systems. Understanding the stability properties of these states is essential for predicting the behavior of optical systems under various conditions and perturbations. Linear stability analysis provides a rigorous mathematical framework for assessing the regions of instability of CW states. By identifying regions of stability and instability, we can gain critical understanding of the underlying dynamics and potential for the emergence of complex phenomena such as pattern formation, soliton generation, and chaos.

Chapter 3

Spatial Dynamics of Stationary Quartic LLE

This chapter describes the spatial dynamics of stationary solutions to the quartic LLE. These dynamics often involve the formation of coherent structures, such as bright and dark solitons, or other localized structures. Bright solitons correspond to localized peaks in the intensity profile of the wave and dark solitons correspond to localized dips in the intensity. Dark solitons form when the dispersive effects counteract the tendency of the nonlinear medium to focus light, resulting in a localized region where the optical intensity is lower than the surrounding background. This work expands upon work I was previously a part of in [33]. The spatial eigenvalues for the stationary quartic LLE are derived and shown in the paper and in this chapter. Furthermore, in section 3.1, the evolution of the eigenvalues is shown for different values of the detuning parameter θ.

As mentioned previously in section 1.2, a distinct characteristic of pure quartic solitons are their oscillatory decaying tails. Recall, this is different than the conventional case of only second order dispersion engineered solitons that have exponentially decaying tails. The main point of this chapter is to characterize the regions in which the formation of coherent structures are possible given dominant fourth order dispersion. This can be done by looking at the eigenvalues of the tails of the PQS pulses and seeing when the imaginary parts of these eigenvalues are nonzero [12]. There are others ([32], [31], [24]) that have further conducted bifurcation analysis of coherent structures that arise from the unique dynamics given by the stationary solutions of the LLE with second order dispersion. It was also considered in the quartic LLE [33]. The information presented in this chapter is also used later, in section 4.2, to quantify the interaction of two pulses. We can examine their interaction by looking at the

overlap of two tails of the different pulses, i.e. we want to match two oscillatory decaying functions whose characteristics are given by the spatial eigenvalues.

We are interested in analyzing the dynamics of the stationary solutions of the quartic LLE. For the rest of this report, we will only consider the case of self-focusing, i.e. when $\gamma = 1$. The dynamics differ for the self-defocusing case and most experimental settings also focus on this case. One could view the stationary solutions as "branches" coming off of the S-curve shown in the previous chapter (figure 2.1). Hence, this curve (CW solutions), are the starting point for finding coherent structures.

The fixed points are the CW solutions, E_s, and we wish to analyze the stability of the stationary solutions, that is solutions to the LLE where $\frac{\partial E}{\partial t} = 0$,

$$-(1 + i\theta)E + i|E|^2E + i\beta_4\frac{\partial^4 E}{\partial z^4} + P = 0 \tag{3.1}$$

Using dynamical systems theory, equation (3.1) can be simplified to a system of first-order real ODEs in z, namely

$$\begin{aligned}
E_1 = Real(E) &\longrightarrow d_zE_1 = E_3 \\
E_2 = Imag(E) &\longrightarrow d_zE_2 = E_4 \\
E_3 = d_zE_1 &\longrightarrow d_zE_3 = E_5 \\
E_4 = d_zE_2 &\longrightarrow d_zE_4 = E_6 \\
E_5 = d_z^2E_1 &\longrightarrow d_zE_5 = E_7 \\
E_6 = d_z^2E_2 &\longrightarrow d_zE_6 = E_8 \\
E_7 = d_z^3E_1 &\longrightarrow d_zE_7 = \beta_4^{-1}(E_2 + \theta E_1 - E_1(E_1^2 + E_2^2)) \\
E_8 = d_z^3E_2 &\longrightarrow d_zE_8 = \beta_4^{-1}(-E_1 + \theta E_2 - E_2(E_1^2 + E_2^2) + P)
\end{aligned}$$

Letting $y(z) = [E_1, ..., E_8]^T$, it is possible to cast the above system in the form $y'(z) = f(y(z); \theta, P, \beta_4)$ which linearized around the CW solution of $y_0 = [a, b, 0, 0, 0, 0, 0, 0]$ where $E_s = a + ib$, is

$$y'(z) = \mathcal{J}(y_0)y(z) + \mathcal{O}(y^2(z)) \tag{3.2}$$

The eigenvalues of the Jacobian matrix $\mathcal{J}(y_0)$ determine whether the tails of the stationary state are oscillatory or monotonic [33]. This leads to the characteristic equation:

$$\beta_4^2\lambda^8 + \beta_4\lambda^4(4|E_s|^2 - 2\theta) + (1 + \theta^2 - 4\theta|E_s|^2 + 3|E_s|^4) = 0 \tag{3.3}$$

that has eight roots. This characteristic equation is the same for the purely second order dispersion case for the LLE with the substitution $\lambda \to \sqrt{i\lambda}$, resulting in four eigenvalues. The eight eigenvalues of equation (3.3) are

$$\lambda_{1,2,3,4,5,6,7,8} = \pm\sqrt{\pm\sqrt{\frac{1}{\beta_4}\left(\theta - 2|E_s|^2 \pm \sqrt{|E_s|^4 - 1}\right)}}$$

Let q_1, q_2, k_1 be positive real numbers and take $\beta_4 = 1$. Similar studies can be done for the case when $\beta_4 = -1$, so we only present the case when $\beta_4 = 1$. There are four qualitatively different eigenvalue configurations:

1. There are two quartets of complex eigenvalues:

$$\lambda_{1,2,5,6} = \pm q_1 \pm iq_1$$

$$\lambda_{3,4,7,8} = \pm q_2 \pm iq_2$$

2. There are two quartets of complex eigenvalues:

$$\lambda_{1,2,3,4} = \pm q_1 \pm ik_1$$

$$\lambda_{5,6,7,8} = \pm k_1 \pm iq_1$$

3. Four eigenvalues are real and four are imaginary:

$$\lambda_{1,2} = \pm q_1$$

$$\lambda_{3,4} = \pm q_2$$

$$\lambda_{5,6} = \pm iq_1$$

$$\lambda_{7,8} = \pm iq_2$$

4. Two eigenvalues are real, two are imaginary, and there is one quartet of complex eigenvalues:

$$\lambda_{1,2} = \pm q_1$$

$$\lambda_{3,4,7,8} = \pm q_2 \pm iq_2$$

$$\lambda_{5,6} = \pm iq_1$$

Numerical simulations were run where $\theta = 3$ is fixed and $|E_s|^2$ is increased from 0 to 5. The eigenvalues, from of the quartic LLE, are plotted in figure 3.1. Each color corresponds to a different eigenvalue (black is repeated). More detailed work is shown in section 3.1 in looking at these regions and where these eigenvalues lie on the "S-shape" bifurcation diagram in figure 2.1.

Table 3.1 lists the four cases of the different eigenvalue configurations, along with the names of the eight-dimension stability classification, and their corresponding region numbers.

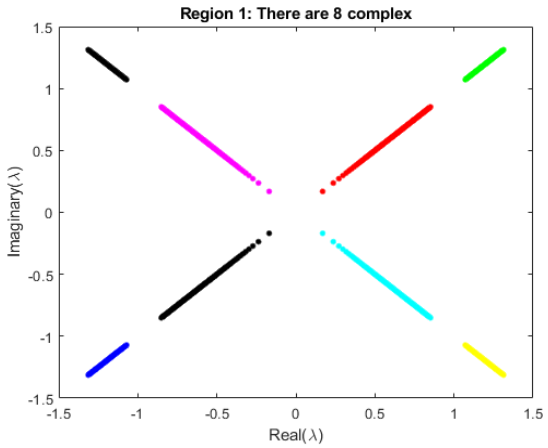

(a) Region 1

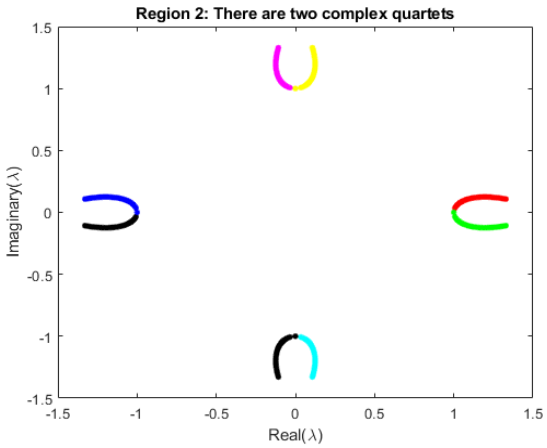

(b) Region 2

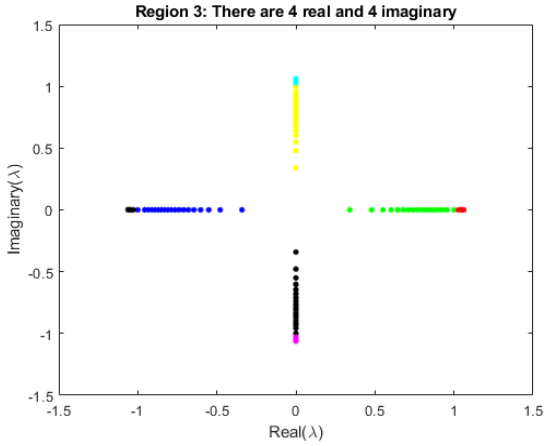

(c) Region 3

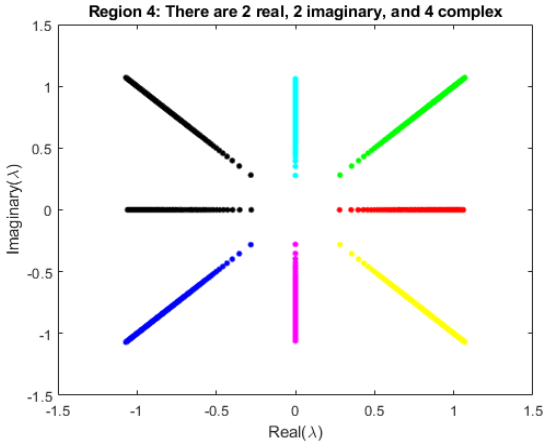

(d) Region 4

Figure 3.1: The four regions of possible organization of the spatial eigenvalues λ

As $|E_s|^2$ increases, the eigenvalues evolve and may transition between regions. During such evolutions, bifurcations occur. Transitioning from region 1 to 2 yields four distinct complex eigenvalues, each with a multiplicity of two, arising from eigenvalue interactions within the complex plane. From region 2 to 3, there are four distinct eigenvalues: two real and two imaginary each with a multiplicity of two caused by the eigenvalues combining along the real and imaginary axis. Moving from region 3 to 4 results in five distinct eigenvalues: two real, two imaginary, and four at $\lambda = 0$, arising from the convergence of four eigenvalues to the origin. Transitioning from region 4 to 1 yields five distinct eigenvalues: four complex and

$(\lambda_{1,2}, \lambda_{3,4}, \lambda_{5,6}, \lambda_{7,8})$	Name	Region
$(\pm q_1 \pm i q_1, \pm q_2 \pm i q_2, \pm q_1 \mp i q_1, \pm q_2 \mp i q_2)$	Quatri focus	1
$(\pm q_1 \pm i k_1, \pm q_1 \mp i k_1, \pm k_1 \pm i q_1, \pm k_1 \mp i q_1)$	Quatri focus	2
$(\pm q_1, \pm q_2, \pm i q_1, \pm i q_2)$	Double saddle-Double center	3
$(\pm q_1, \pm q_2 \pm i q_2, \pm i q_1, \pm q_2 \mp i q_2)$	Saddle-Center-Double focus	4

Table 3.1: Summary table of different eigenvalues as $|E_s|^2$ increases

four at $\lambda = 0$. Finally, transitioning from region 1 to 3 results in all eigenvalues being zero, i.e., $\lambda = 0$ with a multiplicity of 8.

In comparison to the second-order dispersion case of the LLE, there exist more regions in the parameter space that result in the generation of coherent structures. In the quartic LLE, regions 1, 2, and 4 exhibit the emission of complex eigenvalues, enabling the presence of oscillatory tails in the stationary states. This corresponds to the lower and upper part of the S-curve for the CW solutions. Hence, the presence of higher-order dispersion could potentially increase the occurrence of coherent structures, as indicated by the complex dynamics exhibited by the spatial eigenvalues.

3.1. Tracking Spatial Eigenvalues for Different Values of θ

This section demonstrates the effect of the value θ on the spatial eigenvalues. As in [31], CW states of the LLE and their spatial eigenvalue configuration can be tracked for several values of θ. The critical point of the S-cuve occurs when $\theta = \sqrt{3}$ and from the linear stability analysis in section 2.1, there is also a critical value of $\theta = 2$. Hence, there are four different cases to consider for the different values of θ; (i) $\theta = 1.5 < \sqrt{3}$, (ii) $\sqrt{3} < \theta = 1.75$, (iii) $\theta = 2$, (iv) $2 < \theta = 4$.

1. Case (i): $\theta = 1.5$

   There is one bifurcation point that occurs when $|E_s|^2 = 1$. There are four unique eigenvalues with multiplicity 2 of type $\lambda_{1,2,3,4} = \pm q \pm iq$ at this point. As $|E_s|^2$ increases,

the evolution is as follows: Region 2 → Bifurcation at $|E_s|^2 = 1$ → Region 1. The arrangement of eigenvalues is shown in figure 3.2 as $|E_s|^2$ increases.

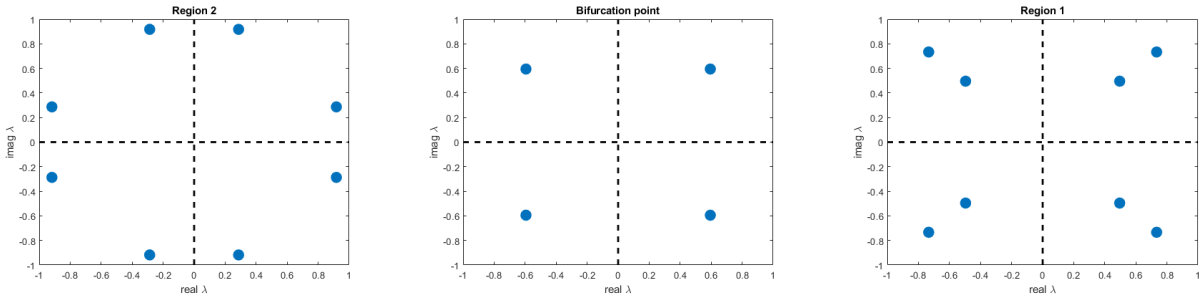

(a) Region 2: Quatri-focus (b) Bifurcation at $|E_s|^2 = 1$. (c) Region 1: Quatri-focus

Figure 3.2: Case (i) when $\theta < \sqrt{3}$

2. Case (ii): $\theta = 1.75$

   There are three points of bifurcation that occur when $|E_s|^2 = 1, 1.0833, 1.25$. For the first bifurcation point, there are four unique eigenvalues with multiplicity 2 of the type $\lambda_{1,2,3,4} = \pm q \pm iq$. For the second bifurcation point, there are four complex eigenvalues of the type $\lambda_{1,2,3,4} = \pm q \pm iq$ and four zero eigenvalues. For the third bifurcation point, there are four complex eigenvalues of the type $\lambda_{1,2,3,4} = \pm q \pm iq$ and four zero eigenvalues. As $|E_s|^2$ increases, the evolution is as follows: Region 2 → Bifurcation at $|E_s|^2 = 1$ → Region 1 → Bifurcation at $|E_s|^2 = 1.0833$ → Region 4 → Bifurcation at $|E_s|^2 = 1.25$ → Region 1. The arrangement of eigenvalues is shown in figure 3.3 as $|E_s|^2$ increases.

3. Case (iii): $\theta = 2$

   There are two points of bifurcation that occur when $|E_s|^2 = 1, 1.6665$. For the first bifurcation point, all eigenvalues equal zero. For the second bifurcation point, there are four complex eigenvalues of the type $\lambda_{1,2,3,4} = \pm q \pm iq$ and four zero eigenvalues. As $|E_s|^2$ increases, the evolution is as follows: Region 2 → Bifurcation at $|E_s|^2 = 1$ → Region 4 → Bifurcation at $|E_s|^2 = 1.6665$ → Region 1. The arrangement of eigenvalues is shown in figure 3.4 as $|E_s|^2$ increases.

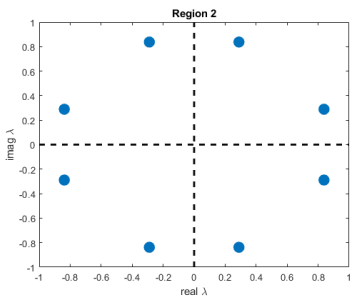

(a) Region 2: Quatri focus

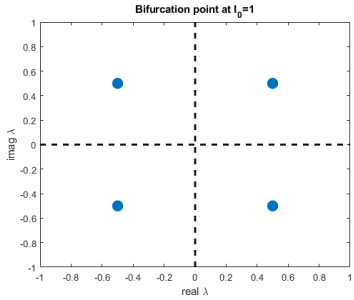

(b) Bifurcation at $|E_s|^2 = 1$.

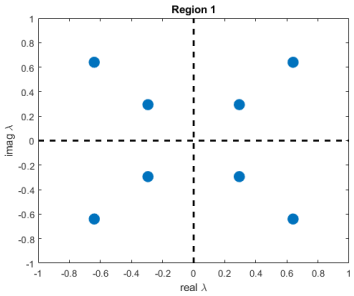

(c) Region 1: Quatri focus

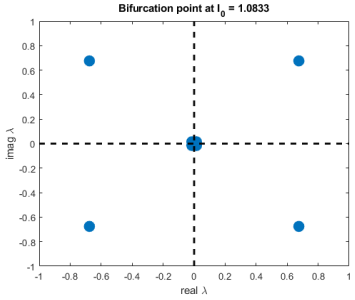

(d) Bifurcation at $|E_s|^2 = 1.0833$.

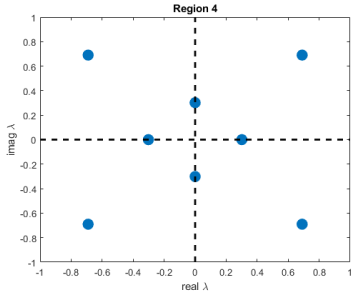

(e) Region 4: Saddle-center-2 focus

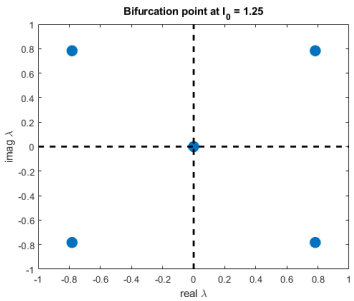

(f) Bifurcation at $|E_s|^2 = 1.25$.

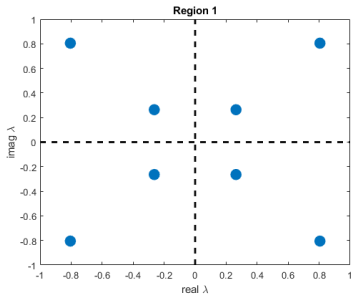

(g) Region 1: Quatri focus

Figure 3.3: Case (ii) when $\sqrt{3} < \theta < 2$

4. Case (iv): $\theta = 4$

   There are three points of bifurcation that occur when $|E_s|^2 = 1, 1.4648, 3.8685$. For the first bifurcation point, there are four unique eigenvalues with multiplicity 2 of the type $\lambda_{1,2,3,4} = \pm q, \pm iq$. For the second bifurcation point, there are four unique eigenvalues of the type $\lambda_{1,2,3,4} = \pm q, \pm iq$ and four zero eigenvalues. For the third bifurcation, there are four complex eigenvalues of the type $\lambda_{1,2,3,4} = \pm q \pm iq$ and four zero eigenvalues. As $|E_s|^2$ increases, the evolution is as follows: Region 2 $\rightarrow$ Bifurcation at $|E_s|^2 = 1 \rightarrow$ Region 3 $\rightarrow$ Bifurcation at $|E_s|^2 = 1.4648 \rightarrow$ Region 4 $\rightarrow$ Bifurcation at $|E_s|^2 = 3.8685$

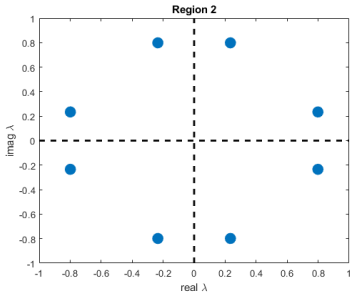

(a) Region 2: Quatri focus

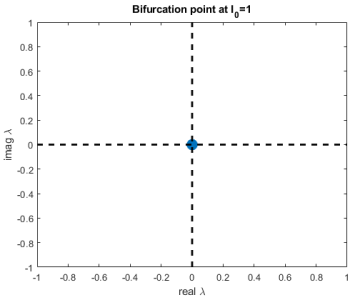

(b) Bifurcation at $|E_s|^2 = 1$.

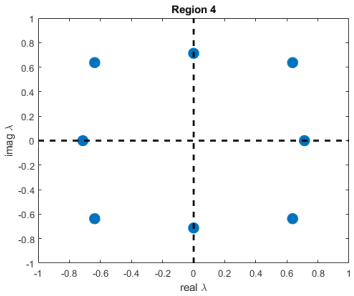

(c) Region 4: Saddle-center-2 focus

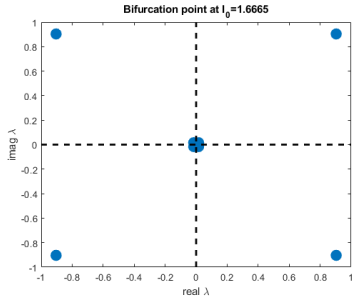

(d) Bifurcation at $|E_s|^2 = 1.6665$.

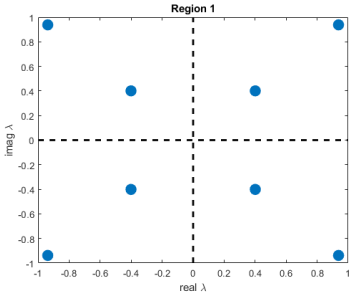

(e) Region 1: Quatri focus

Figure 3.4: Case (iii) when $\theta = 2$

$\rightarrow$ Region 1. Also note that this is the only case in which we get eigenvalues in region 3. The arrangement of eigenvalues is shown in figure 3.5 as $|E_s|^2$ increases.

In conclusion, the exploration of the spatial dynamics of stationary quartic Lugiato-Lefever equations (LLE) and the tracking of spatial eigenvalues across various detuning parameter values provide invaluable insights into the intricate behaviors of nonlinear optical systems with fourth-order dispersion. Compared to the quadratic LLE, there are increased opportunities for the generation of coherent structures due to the unique characteristic of PQSs, namely their oscillatory decaying tails. Through theoretical analysis and computational simulations, this study has shed light on the complex interplay between the detuning parameter and the spatial eigenvalues, revealing intriguing phenomena such as pattern formation and stability transitions. The findings not only deepen our understanding of fundamental nonlinear phenomena but also offer practical implications of photonic devices and

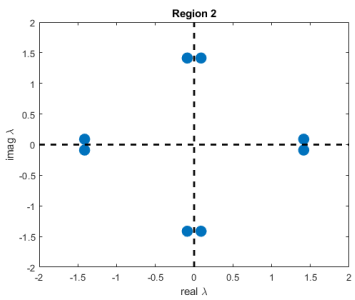

(a) Region 2: Quatri focus

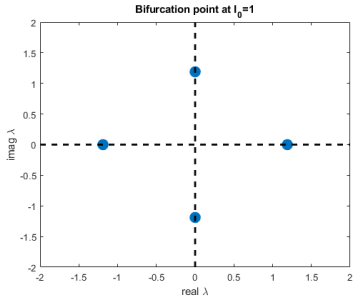

(b) Bifurcation at $|E_s|^2 = 1$.

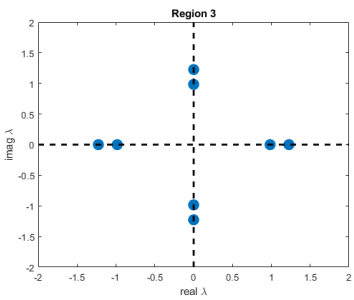

(c) Region 3: 2 saddle-2 center

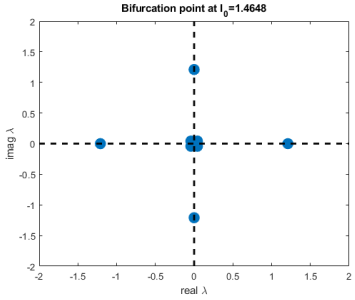

(d) Bifurcation at $|E_s|^2 = 1.4648$.

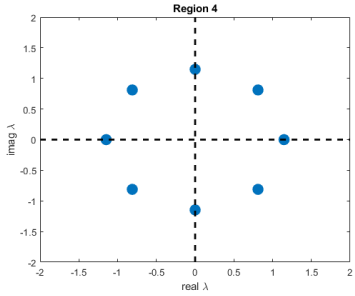

(e) Region 4: Saddle-center-2 focus

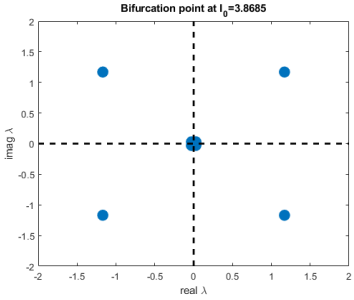

(f) Bifurcation at $|E_s|^2 = 3.8685$.

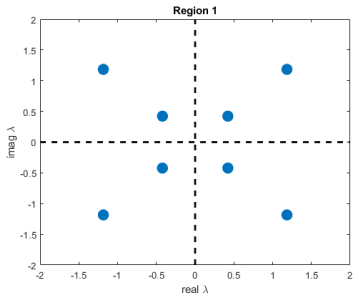

(g) Region 1: Quatri focus

Figure 3.5: Case (iv) when $4 = \theta > 2$

systems. As we continue to delve into the dynamics of nonlinear optical systems, the insights gleaned from this research serve as a foundation for further exploration and innovation.

Chapter 4

Numerical Studies of the LLE with Dominant Quartic Dispersion

The goal of this chapter is to test a variety of different initial conditions for the emergence of coherent structures. The type of initial conditions considered are *sech* function (bright pulse), noisy functions, and $tanh^2$ function (dark pulse). We consider both cases when $\beta_4 < 0$ and $\beta_4 > 0$ for the first two cases and only positive β_4 for the last case. The interest lies in the long-term behavior of the model and provides valuable insights for the rest of the work presented in the subsequent chapters.

These numerical realizations showcase our exploration into introducing noise into our initial conditions. For inputs of *sech*-type and $tanh^2$-type, the coherent structures observed provide valuable insight into the behavior of the system. It's important to note that not all of this is an exhaustive study. As it relates to the noisy initial condition, we haven't conducted any statistical analysis, nor have we addressed numerical artifacts like aliasing. For instance, in the numerical scheme used for simulations, we integrate the linear part in Fourier space which leads to non-physical filtering. Despite these considerations, these results still offer insights into the emergence of coherent structures, potentially serving as attractors.

The quartic Lugiato-Lefever equation is solved numerically using the split-step fourier method. The construction of split-step fourier method in this regime is well established [1]. Solving the LLE using the split-step fourier method is outlined here [17] and further in the LLE with the effects of higher-order dispersion, Raman scattering, and self-steepening [13]. Given an initial condition, the system updates in time by discretizing the space domain into N equally-spaced fourier modes and splitting equation (1.4) up into two parts. The linear component accounts for loss, detuning, and dispersion and the nonlinear component

accounts for the cubic nonlinearity term. That is

$$\frac{\partial E}{\partial t} = (\mathcal{N} + \mathcal{L})E + P \tag{4.1}$$

$$\mathcal{N} = i|E|^2 \tag{4.2}$$

$$\mathcal{L} = -(1 + i\theta) + i\beta_4 \frac{\partial^4 E}{\partial z^4} \tag{4.3}$$

The nonlinear part, using standard ODE methods, results in the update

$$\frac{\partial E}{\partial t} = \mathcal{N}E \tag{4.4}$$

$$\Rightarrow E(t + \Delta t, z) = exp(\Delta t \mathcal{N})E(t, z) \tag{4.5}$$

$$E(t + \Delta t, z) = exp(i\Delta t|E(t, z)|^2)E(t, z) \tag{4.6}$$

For the linear part, we first make a change of variables since the pump power P is constant. We want to make the substitution

$$E(t, z) = A(t, z) + \frac{P}{(1 + i\theta)} \tag{4.7}$$

So that

$$\frac{\partial A}{\partial t} = \left[-(1 + i\theta) + i\beta_4 \frac{\partial^4}{\partial z^4} \right] A \tag{4.8}$$

The linear part is solved by means of finite fast fourier transform with the solution being in the fourier domain where k are the fourier wavenumbers. Let $\tilde{A}(t, k) = \mathcal{F}(A(t, z))$ so

$$\frac{\partial}{\partial t}\tilde{A}(t, k) = \mathcal{F}\left[\left(-(1 + i\theta) + i\beta_4 \frac{\partial^4}{\partial z^4} \right) A(t, z) \right] \tag{4.9}$$

$$= \left[-(1 + i\theta) + i\beta_4 (ik)^4 \right] \tilde{A}(t, k) \tag{4.10}$$

$$\frac{\partial}{\partial t}\tilde{A}(t, k) = \left[-(1 + i\theta) + i\beta_4 k^4 \right] \tilde{A}(t, k) \tag{4.11}$$

$$\Rightarrow \tilde{A}(t + \Delta t, k) = exp(\Delta t(-(1 + i\theta) + i\beta_4 k^4))\tilde{A}(t, k) \tag{4.12}$$

So that the update in the for the linear part is

$$A(t+\Delta t,z)=\mathcal{F}^{-}1\left[exp(\Delta t(-(1+i\theta)+i\beta_4k^4))*\mathcal{F}(A(t+\Delta t,z))\right] \tag{4.13}$$

Using the substitution in equation (4.7), we obtain the update in E, that is

$$E(t+\Delta t,z)=\mathcal{F}^{-}1\left[exp(\Delta t(-(1+i\theta)+i\beta_4k^4))*\mathcal{F}\left(E(t+\Delta t,z)-\frac{P}{1+i\theta}\right)\right]+\frac{P}{1+i\theta} \tag{4.14}$$

Combining equation (4.6) and equation (4.14) gives the numerical solution update

$$E(t+\Delta t,z)=\mathcal{F}^{-}1\left[exp(\Delta t(-(1+i\theta)+i\beta_4k^4))*\mathcal{F}\left(exp(i\Delta t|E(t,z)|^2)E(t,z)-\frac{P}{1+i\theta}\right)\right]+\frac{P}{1+i\theta} \tag{4.15}$$

where the part in red is from the nonlinear update. The system either devolves into chaos or reaches a steady state solution consisting of pulse-like structures. If steady state is reached and the system does not become chaotic, the final numerical solutions are taken at some time T. This is determined when the L^2 norm of the current state compared with the previous states is sufficiently small ($< 10^{-8}$), i.e.

$$|E(T,z)-E(t,z)|^2< 10^{-8} \tag{4.16}$$

The quartic LLE is posed on the line $[-L,L]$, where $2L$ is the total domain length. Here, there is periodic boundary conditions but we make L large enough ($L=40$) so there is no interaction of structures on the boundary for the case of *sech*-type and $tanh^2$-type initial conditions. This is to mimic the problem being posed on an infinite line. However, for the case of noisy initial conditions, the boundaries are just periodic. The parameters θ, P, β_4 are given initially. The time step is taken to be $\Delta t = 0.001$. The number of fourier modes, N, is in most cases taken to be $N = 1024$. In chapter 6 when the domain size is smaller, $N = 512$ is sufficient. Algorithm 1 demonstrates some pseudocode of the split-step fourier

method for the quartic LLE whose update formula is given by equation (4.15). The FFT and IFFT functions refer to the fast fourier transform and the inverse fast fourier transform, respectively. The initial condition is discussed in the next section (section 4.1) as we consider a variety of initial conditions.

Algorithm 1 Split-step fourier method for quartic LLE

Require: $u_0 = E(0, z)$ ▷ Initial condition
  for $m = 0 : \Delta t : T$ **do**
    $u_1 = exp(i\Delta t * \text{abs}(u_0)^2) * u_0 - P/(1 + i\theta)$
    $u_2 = \text{FFT}(u_1)$
    $u_3 = exp(\Delta t(-(1 + i\theta) + i\beta_4 k^4)) * u_2$
    $u_4 = \text{IFFT}(u_3) + P/(1 + i\theta)$
    $u_0 = u_4$
  end for

4.1. Numerical Simulations of Different IC

The goal of this section is to test a variety of initial conditions to observe the emergence of coherent structures or the system devolving into chaos. The subsequent sub-sections are for the different cases when the sign of the fourth-order dispersion parameter is negative or positive. The intention is the see the role of the sign of the dispersion parameter as different structures exist for different values. We will consider a range of initial conditions:

i Case 1: The initial condition is taken to be a single bright pulse of the form:

$$E(0, z) = a + bsech(cz)$$

where a is taken to be the CW solution and b and c, in this case, are taken to be

$$b = \sqrt{2\theta}(\zeta + i\sqrt{1 - \zeta^2}) \text{ where } \zeta = \frac{\sqrt{8\theta}}{P\pi}$$
$$c = \sqrt{\theta}$$

The values for b and c are taken from [27]. We consider this case for both $\beta_4 < 0$ and $\beta_4 > 0$.

ii Case 2: Starting with the constant solution from the CW solutions and adding on some noise:

$$E(0, z) = a + re^{i\tilde{z}}$$

where r is the amplitude of the noise taken to be some real number such that $r \in [0, 1]$ and $\tilde{z}$ is a random variable whose values are sampled from the standard normal distribution. Essentially, this takes the CW solution and perturbs it, where the perturbation is characterized by values drawn from the standard normal distribution. We consider this case for both $\beta_4 < 0$ and $\beta_4 > 0$.

iii Case 3: This case is only considered when $\beta_4 > 0$. The initial condition is taken to be a single dark pulse of the form

$$E(0, z) = a + tanh^2(z)$$

where a is the CW solution. The form of this initial condition is taken in this way as it provides the simplest case of adding a dark pulse to the background CW state.

4.1.1. Emergence of Coherent Structures or Chaotic Regimes for the Quartic LLE with $\beta_4 < 0$

The first case considered is Case 1 where the initial condition is in the form of a single bright pulse. For these simulations, take $\theta = 3$ and $P = 2$. For this initial condition and the parameters taken, we expect to see a variety of behavior from the system. There have been more rigorous studies on the existence and stability of coherent structures ([32], [31], [33], [29]) showing it is possible to obtain single bright pulses and multi-pulse solutions. The

CW solutions exhibit hysteresis behavior where the system transitions between different dynamical regimes as the parameters are varied. The bifurcations from the S-curve can lead to the onset of chaotic behavior. Hysteresis can thus act as a catalyst for the emergence of chaos due to the multiple CW states. Hence, depending on the CW state used in the initial condition, this can lead to very different behavior.

The following figures have the initial condition in the top left and show snapshots over time the behavior of the system. They are progressed in time from left to right, with the final time shown in the last subplot in the bottom right for each figure. Figure 4.1 is an example where initially, the system is given a very intense input with high energy. As the energy spreads out across the domain, it settles to a train of pulses. The CW solution is taken from the bottom part of the S-curve. Figure 4.2 shows how the system appears to be going towards a multi-pulse solution but then devolves into chaos. Here, the CW solution is taken from the middle part of the S-curve where it is unstable. Figure 4.3 is an example of a bright pulse solution. Here, the CW solution is taken from the top part of the S-curve.

These figures (4.1 - 4.3) showcase how starting from a different background state, the system can exhibit different behavior. Although not shown here, through numerical simulations, it is also possible to obtain a single bright pulse as the steady state solution when the CW state is taken from the lower part of the S-curve. However, when taking the initial background state as the middle part of the S-curve, the system will not converge to a steady state solution.

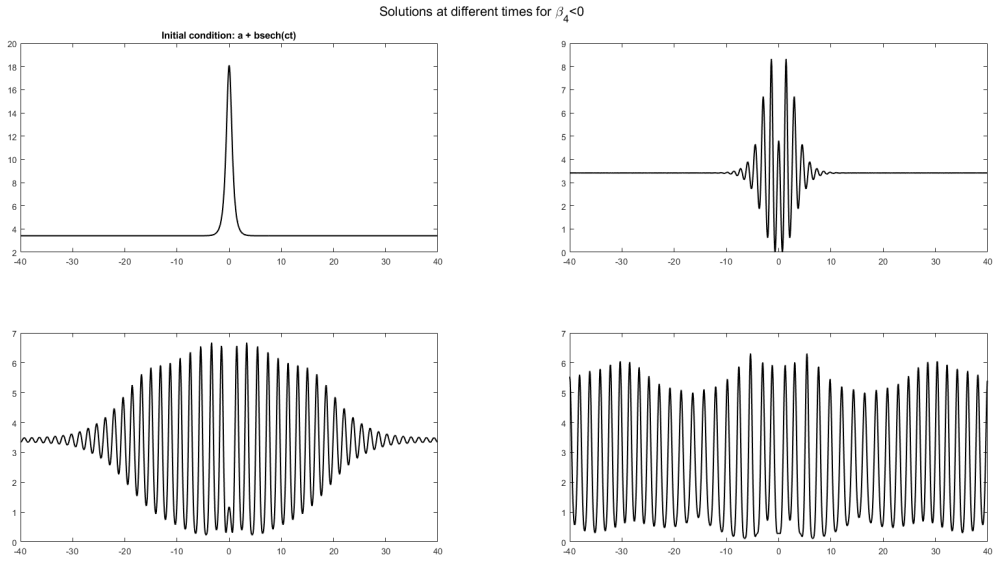

Figure 4.1: Evolution where the constant a is taken from the lower part of the S-curve.

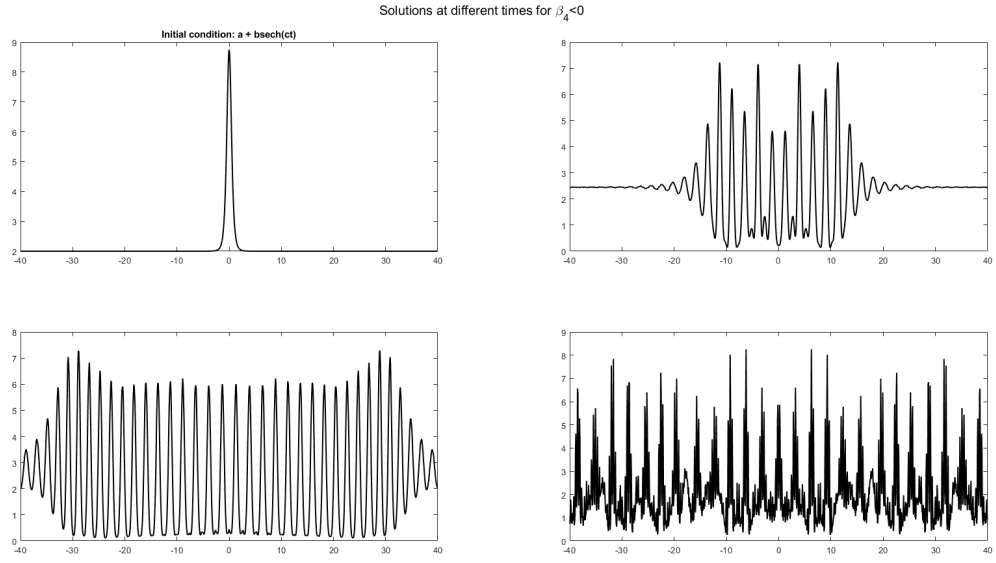

Figure 4.2: Evolution where the constant a is taken from the middle part of the S-curve.

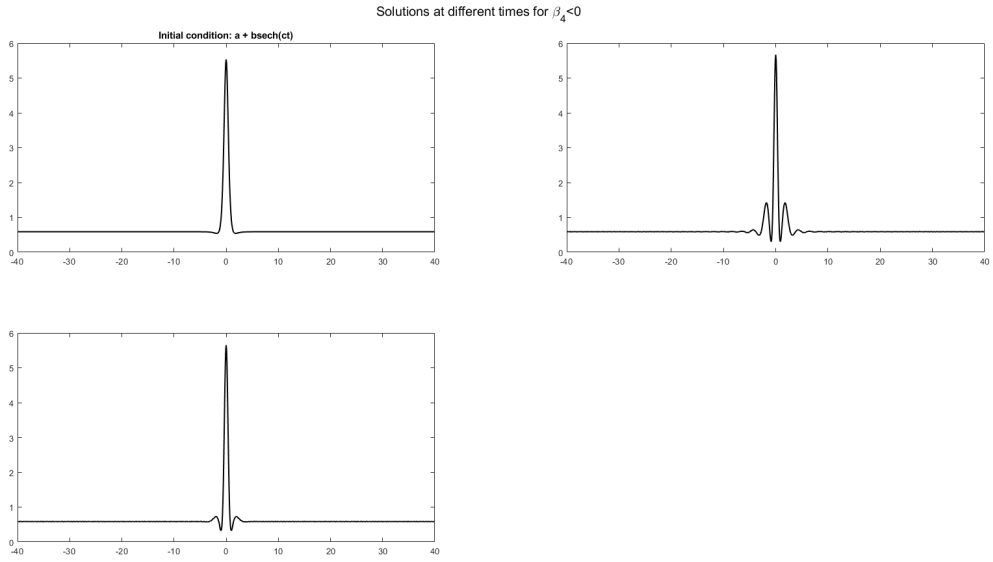

Figure 4.3: Evolution where the constant a is taken from the top part of the S-curve.

The second case considered is where the initial condition is in the form of the CW background state with some noise. The noise is taken from a normal distribution where the mean is the CW solution and the standard deviation is either taken to be small, i.e. $r = 0.1$ or large, i.e. $r = 0.7$. For small noise, most of the behavior we observed, would be that of the CW solution or no coherent structures.

For figure 4.4, we see some of the multi-pulse behavior before the resulting state of the system is quasi-periodic. This was indeed the case for the simulations when a is on the lower or middle part of the S-curve, meaning it is very difficult to obtain pulse-like solutions for this case.

It was observed however, that as we increase the noise, more interesting behavior emerges. For the next two figures (4.5 and 4.6), the initial conditions have large noise and the same mean, meaning we have the same type of solutions but see a different number of bright pulses that emerge because of the randomness of the initial condition. Figure 4.5 stabilizes into four bright pulses and figure 4.6 stabilizes into two bright pulses, each with differing

pulse separation distances. The observation of stable coherent structures with different pulse separation distances and number of pulses was the motivation for section 4.2 and for chapter 5. It would be interesting to do further statistical analysis to see if one could characterize the number of pulses seen in the final steady state solution based on the sampling done in the initial condition for the noise added into the CW state. The background state for these cases was taken from the top part of the S-curve where we see similar behavior as in figure 4.3.

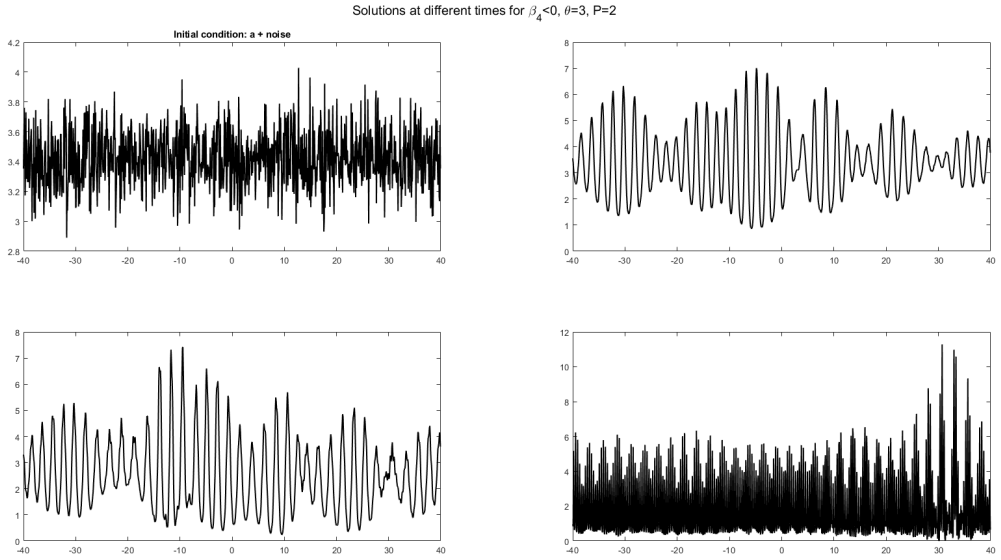

Figure 4.4: Evolution where the constant a is taken from the lower part of the S-curve with small noise

Through numerical observations of starting with inputs of smooth pulse-like functions like *sech*-type or starting with noise, we can see the emergence of coherent structures for the case when $\beta_4 < 0$. This does appear to be dependent on the background state used in the initial condition, as starting with a CW state from the middle part of the S-curve does not result in coherent structures.

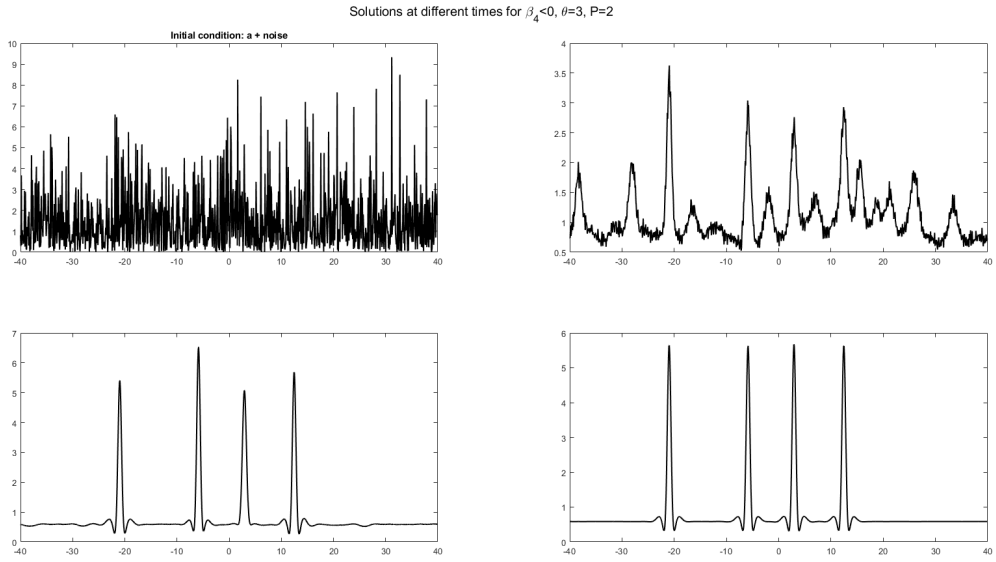

Figure 4.5: Evolution where the constant a is taken from the top part of the S-curve with large noise.

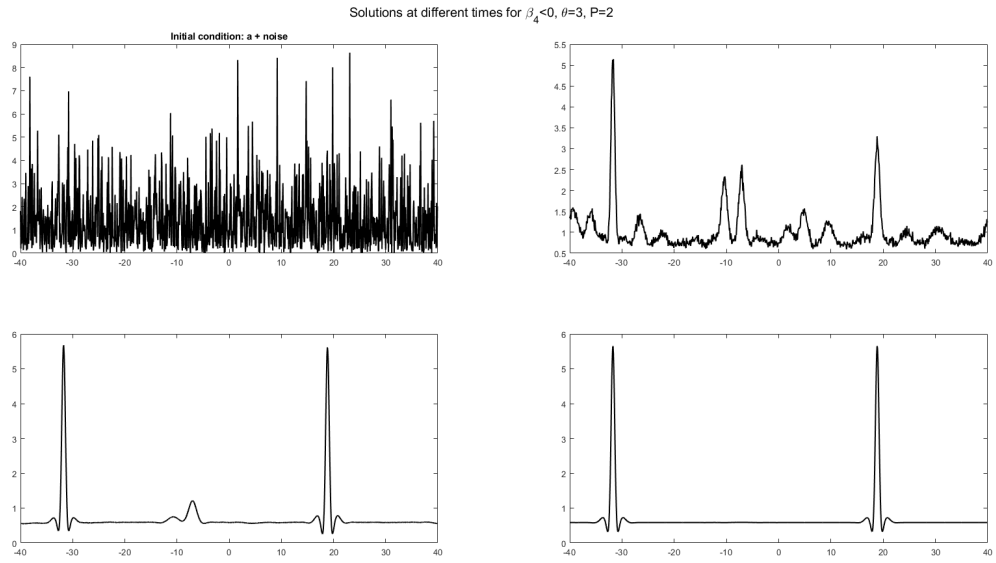

Figure 4.6: Evolution where the constant a is taken from the top part of the S-curve with large noise.

4.1.2. Emergence of Coherent Structures or Chaotic Regimes for the Quartic LLE with $\beta_4 > 0$

We now want to consider the cases of different initial conditions for the case when $\beta_4 > 0$ to observe the possible emergence of coherent structures or other types of behavior in the system. The first case considered is where the initial condition is in the form of a single bright pulse. For figure 4.7, take $\theta = 6$ and $P = 3$ and for figure 4.8, take $\theta = 6$ and $P = 4$. When running this initial condition where the constant a is taken from the middle part of the S-curve, the solution devolves into chaos and doesn't reach a stable state. Figure 4.7 shows how a dark pulse is formed when initially the input is a bright pulse. Also, there is some interesting behavior in the dip of the dark pulse that will be explored more later. However, there is some indication here that for dark pulses, the dips can have compound structures. Figure 4.8 initially appears as if the resulting state would be a multi-pulse solution however, this is a case where the peak of this pulse will very slowly be expanded until the solution becomes constant. This is referred to as a moving front and is like a wall that is expanding. It is further studied in the case of the quadratic LLE in [40] and only appears in the case of positive orders of dispersion.

The second case considered is where the initial condition is in the form of the CW background state with some noise. The noise is taken from a normal distribution where the mean is the CW solution. The parameters are taken to be $\theta = 6$ and $P = 3$. For this case, most of the behavior observed would be that the solution would become constant as time went on. For a small amount of noise, that is when $r = 0.01$, some dark pulse solutions could be found which is shown in figure 4.9. This figure shows dark pulses forming with more compound structures in their dips. This case is particularly interesting since the noise is taken to be quite small but with resulting interesting behavior. In figure 4.10, the standard deviation is taken to be $r = 0.4$. In this figure, it is shown that adding in more noise still results in dark pulses. An interesting characteristic of the dark pulses compared to

the bright pulses, are the structures forming at the dips of the pulses. There has been some very recent work over studying these structures [14] in the NLSE with second and fourth order dispersion.

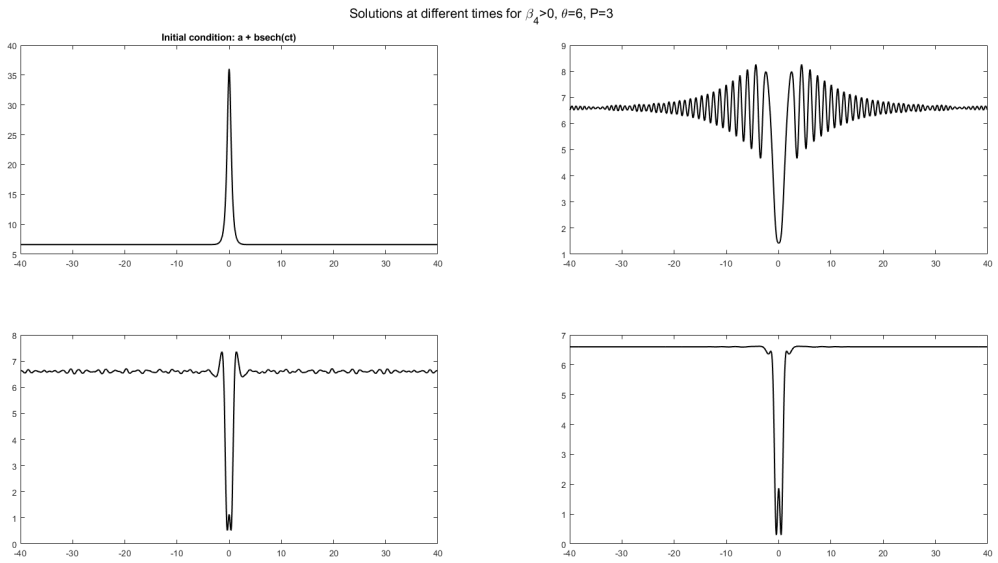

Figure 4.7: Evolution where the constant a is taken from the bottom part of the S-curve.

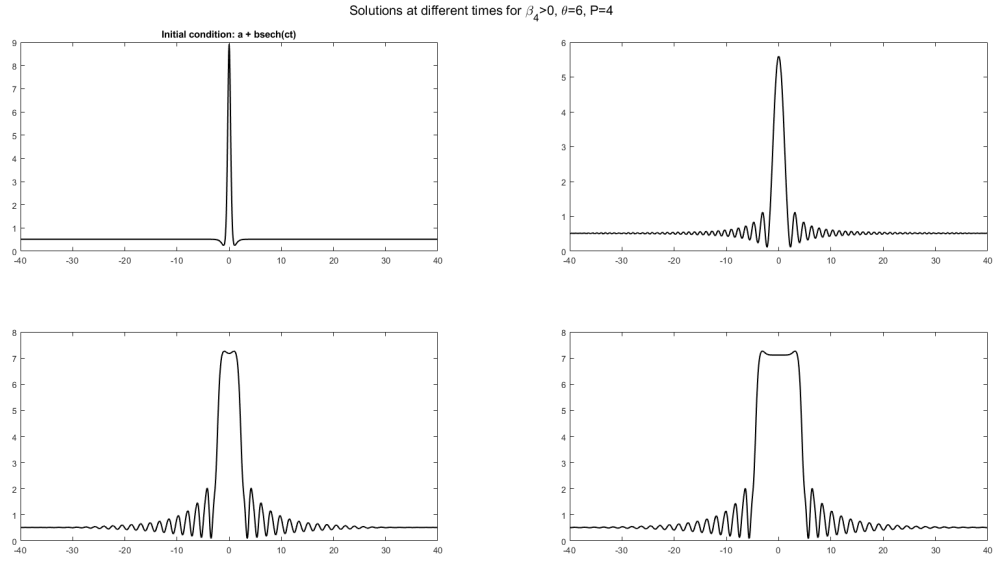

Figure 4.8: Evolution where the constant a is taken from the top part of the S-curve.

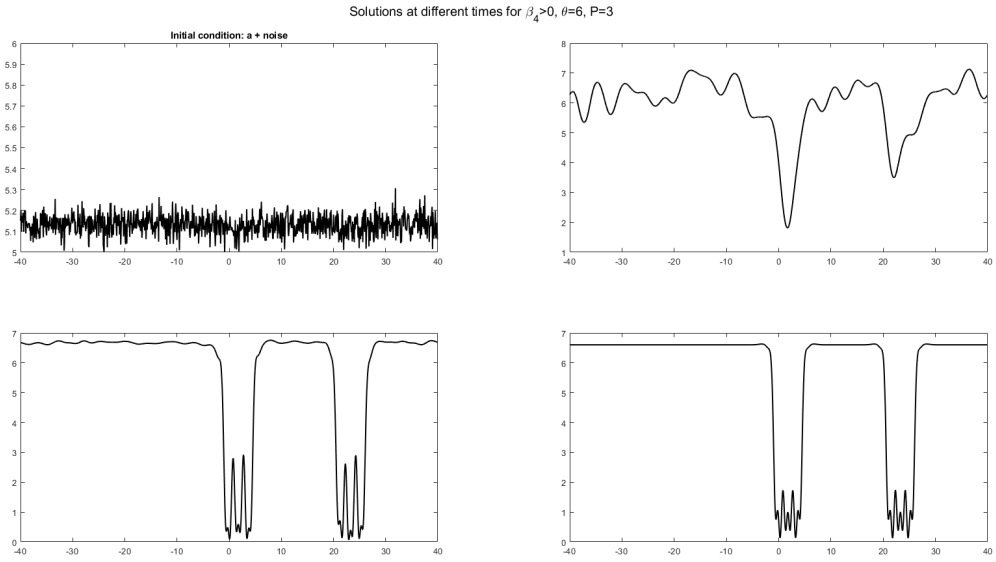

Figure 4.9: Evolution of solution where the constant a is taken from the middle part of the S-curve with the standard deviation taken as very small (0.01)

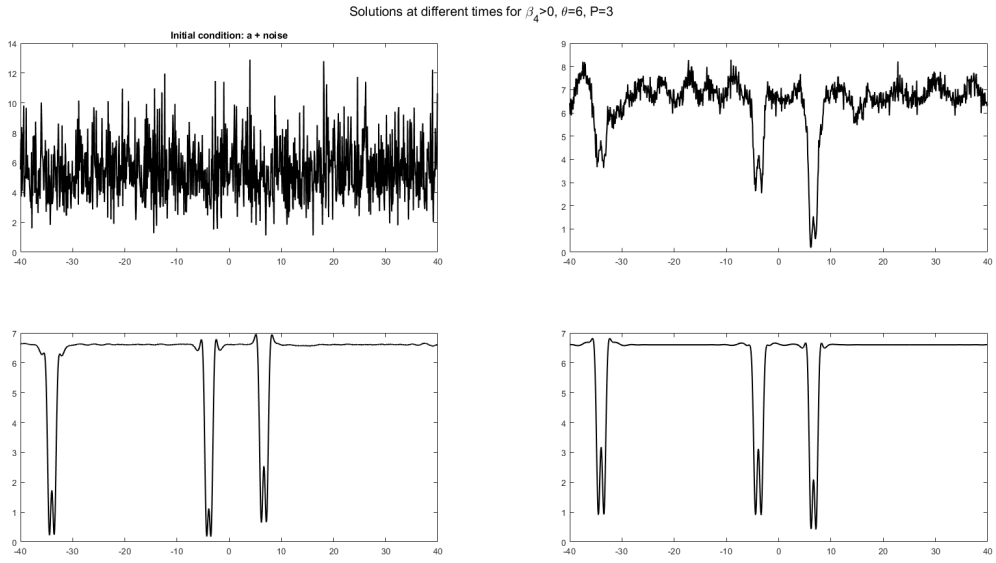

Figure 4.10: Evolution of solution where the constant a is taken from the middle part of the S-curve with the standard deviation taken to be 0.4.

In addition for figures 4.9 and 4.10, the background state is taken from the middle part of the S-curve. Although not shown in chapter 2, changing the sign of the dispersion parameter

results in different stability dynamics of the CW solution. When the dispersion parameter is positive, $\beta_4 > 0$, the middle branch is stable, thus resulting in the dark pulse train seen in the figures.

The last case considered is starting with a dark pulse as the initial condition. As shown in figure 4.11, the behavior exhibited is similar as seen in figure 4.8 as the solution is a moving front. It is also interesting to note that the pulse flips to form this front. These investigations have only scratched the surface and are open to further exploration.

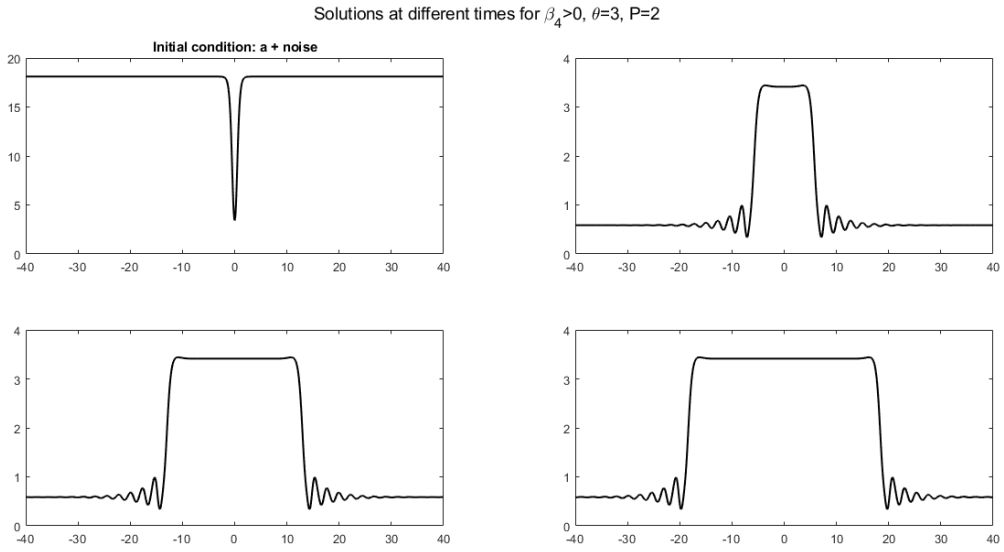

Figure 4.11: Evolution where the constant a is taken from the lower part of the S-curve.

4.2. Generation of Double Pulse Solutions

The inspiration for finding double pulse solutions comes from figure 4.5 and further numerical experiments where it was observed that there were a different kinds of double pulse solutions the system could produce. In doing more simulations with noisy initial conditions, you can find different number of pulse solutions by controlling the amount of noise in the initial condition in a small window. This can be seen in figure 4.12. Sometimes, the system would become chaotic and sometimes the system would decay to a constant

solution as shown in the previous section. This is contingent on the parameter values of the system, i.e. θ, β_4 and P. The goal for this section is to see how to generate a set of stable and unstable double pulse solutions for given parameter values where the system would not devolve into chaos.

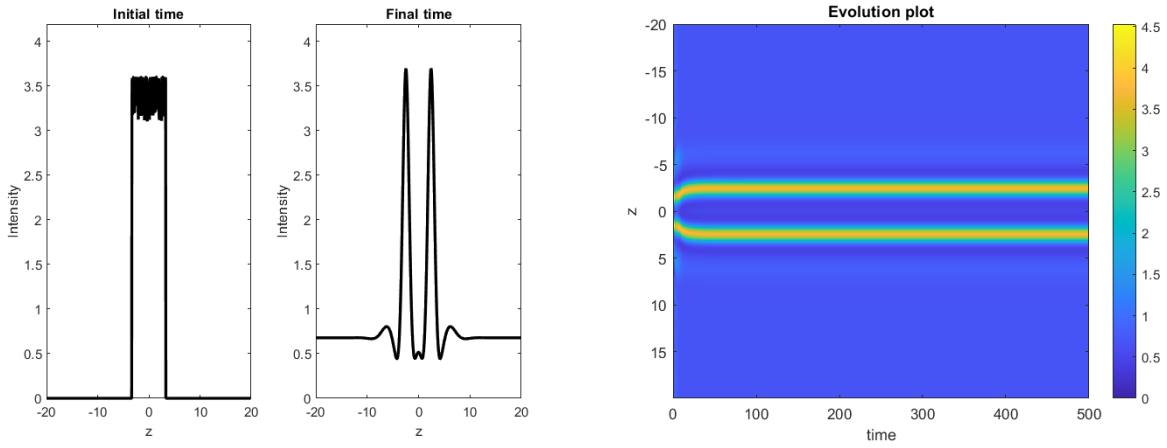

Figure 4.12: Double pulse solution emerging from localized noise

Section 4.1.2 considers the case when $\beta_4 > 0$, but for the rest of this report, we will only consider when $\beta_4 < 0$. Initially, we generate a single pulse by starting with an initial condition of the form:

$$E(0,z) = \begin{cases} E_s + \tilde{E}(z) & \text{if } z \leq |\omega| \\ 0 & \text{if } z > |\omega| \end{cases} \tag{4.17}$$

where E_s is the CW solution and $\tilde{E}(z) = re^{i\phi(z)}$ such that $r \in [0,1]$ is a parameter that represents the amplitude of the noise and $\phi(z)$ is a normal random variable. The parameter ω is the size of the window. An example of this is shown in figure 4.13.

Next, we want to construct the initial conditions of two pulses. The goal is to find all double pulse solutions that satisfy the stationary quartic LLE, that is:

$$-(1+i\theta)E + i|E|^2E + i\beta_4\frac{\partial^4 E}{\partial z^4} + P = 0 \tag{4.18}$$

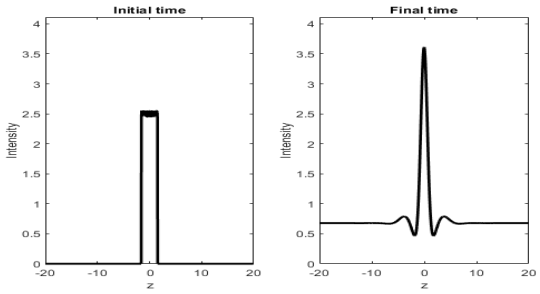

Figure 4.13: Starting with localized noise, the solution evolves in time settling on a single pulse solution.

Assume E(z) is the single pulse solution of the above equation (final time shown in figure 4.13). The double pulse solutions can be formulated in the following way:

$$E_d(0, z; k) = E_+(z) + E_-(z) - E_s \tag{4.19}$$

where $E_+(z) = E(z + k)$ and $E_-(z) = E(z - k)$. The parameter k is a real number that represents the shift to the left or right of the single pulse solution ($k = n\Delta z, n \in \mathbb{Z}$). This is shown in figure 4.14.

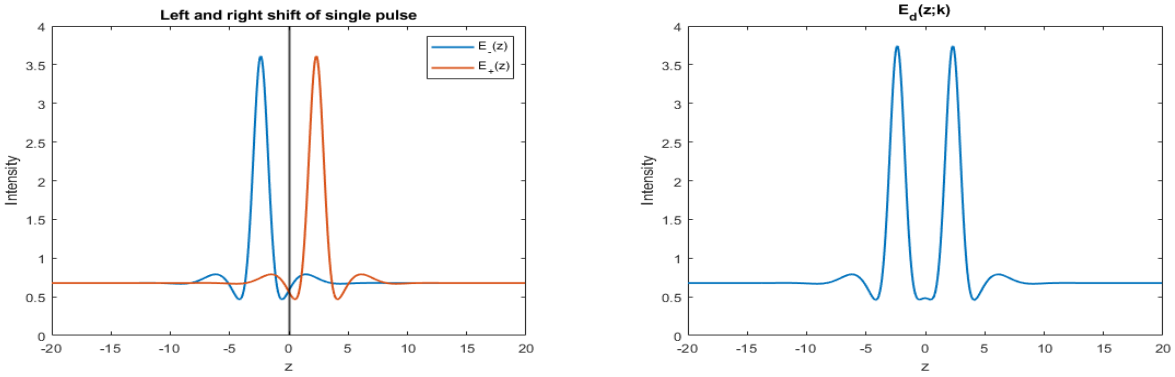

(a) Shifted single pulses (b) Example initial condition

Figure 4.14: Construction of initial condition for finding double pulse solutions

The parameters used for the simulation are $\theta = 2.2$, P=1.5, $\beta_4 = -1/4$, L=40, and N=512. The distance between the pulses went from k=5 to around k=50. The initial condition for equation (4.18) is given by equation (4.19) for a certain k. Initially, the pulses are close together and as k increases, the distance between the pulses increases. We then

want to see the final steady state solution as the distance between the two pulses is increased in the initial condition.

The interaction of the pulses can be regarded by looking at the overlap of the tails of the two pulses. The spatial dynamics of the stationary quartic LLE, whose spatial eigenvalues are from equation (3.3), can be used to find the consecutive separation distance between double pulse solution states. The spatial eigenvalues from the stationary problem that has the smallest negative real part is $\lambda_c = -0.8282 + 1.1949i$ which gives the approximate rate of decay of the oscillatory tails (real λ_c). After a certain distance apart the oscillatory tails of the two pulses don't interact and the two pulses can be regarded as two single pulses existing on the same domain.

From [30], the wavelength of the oscillatory decaying tails is given by

$$\lambda_0^{\text{tails}} = \frac{\pi}{Imag(\lambda_c)} \tag{4.20}$$

If d_i is the distance between the two pulses, then $\Delta d_i = d_{i+1} - d_i$, which is the change of the separation distances between consecutive unstable and stable double pulse solutions. This value should be $\Delta d_i \approx \lambda_0^{\text{tails}}$ and as the distance between pulses grows larger, than $\Delta d_i \to \lambda_0^{\text{tails}}$.

The stability of the double pulse solutions is found from the spectrum of linearization of the double pulse solution. Letting $E = u_r + iu_i$, then the stationary quartic LLE is equivalent to solving:

$$-u_r + \theta u_i - u_i u_r^2 - u_i^3 - \beta_4 \frac{\partial^4 u_i}{\partial z^4} + P = 0 \tag{4.21}$$

$$-u_i - \theta u_r + u_r^3 + u_i^2 u_r + \beta_4 \frac{\partial^4 u_r}{\partial z^4} = 0 \tag{4.22}$$

This system is nonlinear, so the stability of the double pulse solution is found by looking at the eigenvalues of the Jacobian matrix evaluated at the double pulse solution. The Jacobian matrix is defined as

$$J(u_r, u_i) = \begin{bmatrix} -1 - 2u_i u_r & \theta - u_r^2 - 3u_i^2 - \beta_4 \frac{\partial^4}{\partial z^4} \\ -\theta + 3u_r^2 + u_i^2 + \beta_4 \frac{\partial^4}{\partial z^4} & -1 + 2u_i u_r \end{bmatrix} \tag{4.23}$$

When numerically solving for the quartic LLE, we split the space domain, z, into N equally spaced fourier modes: $z_j : z_j = 2L/N, j = 0, ..., N-1$. We solve the stationary quartic LLE on z_j and by using the fourth derivative spectral differentiation matrix, $D^{(4)}$, to approximate $\frac{\partial^4}{\partial z^4}$. Let $U_r = [u_r(z_0), ..., u_r(z_{N-1})]^T$ and $U_i = [u_i(z_0), ..., u_i(z_{N-1})]^T$, then the Jacobian matrix is defined numerically by

$$J(U_r, U_i) = \begin{bmatrix} -I + \text{diag}(-2U_i \cdot U_r) & \text{diag}(\theta - U_r^2 - 3U_i^2) - \beta_4 D^{(4)} \\ \text{diag}(-\theta + 3U_r^2 + U_i^2) + \beta_4 D^{(4)} & -I + \text{diag}(2U_i \cdot U_r) \end{bmatrix} \tag{4.24}$$

where $U_r^2 = [u_r(z_0)^2, ..., u_r(z_N - 1)^2]$ and similarly for U_i^2.

Numerically, U_r, U_i is a Nx1 vector where N is the number of fourier nodes. In this way, we are able to find both the (spectrally) stable and unstable double pulse solutions, that is by looking at the spectrum of the linearization, one can identify the Jacobian matrix, J, and find its eigenvalues. The LLE has the property of translation invariance so one of the N eigenvalues will be zero. The solution is spectrally stable if when we linearize about the solution, all the resulting real parts of the eigenvalues are negative. In other words, by looking at the eigenvalue closest to zero, we can determine the stability of the resulting double pulse solution we obtain from solving the equation, using an initial condition shown in 4.14(b). If that eigenvalue's real part is negative, then it is spectrally stable. If it is

positive, we say it is spectrally unstable. An example of the resulting solution and stability is shown in figure 4.15.

Table 4.1 shows the ending solution distances for each of the five solutions found in figure 4.16, Δd_i, and the eigenvalue closest to 0 from the spectrum of linearization of the Jacobian matrix in equation (4.24) called s_0. The anticipated $\Delta d_i = 2.6293$. The step size for this

d_i	Δd_i	s_0
3.281250	—	4.72985 x 10^{-1}
4.84375	1.5625	-1.10729 x 10^{-1}
7.34375	2.5	2.19461 x 10^{-2}
10.15625	2.8125	-2.46265 x 10^{-3}
12.65625	2.5	2.66639 x 10^{-4}

Table 4.1: Separation distance of pulses with L=40 and N=512

problem is $\Delta z = 0.1562$ meaning for this simulation, the difference in the pulse separation distances should be within the range of $\overline{\Delta d_i} = 2.65625 \pm 0.1562$.

Keeping the same set of parameters for θ, P, β_4 but changing L=20 and N=1024 to see if we get a more accurate estimate. The results are shown in table 4.2. The step size for this problem is $\Delta z = 0.0391$ meaning for this simulation its with the range of $\overline{\Delta d_i} = 2.6302 \pm 0.0391$.

d_i	Δd_i	s_0
3.125	—	4.72985 x 10^{-1}
4.882812	1.757821	-1.10729 x 10^{-1}
7.382812	2.5	2.19461 x 10^{-2}
10.117188	2.734376	-2.46265 x 10^{-3}
12.773438	2.65625	2.66643 x 10^{-4}

Table 4.2: Separation distance of pulses with L=20 and N=1024

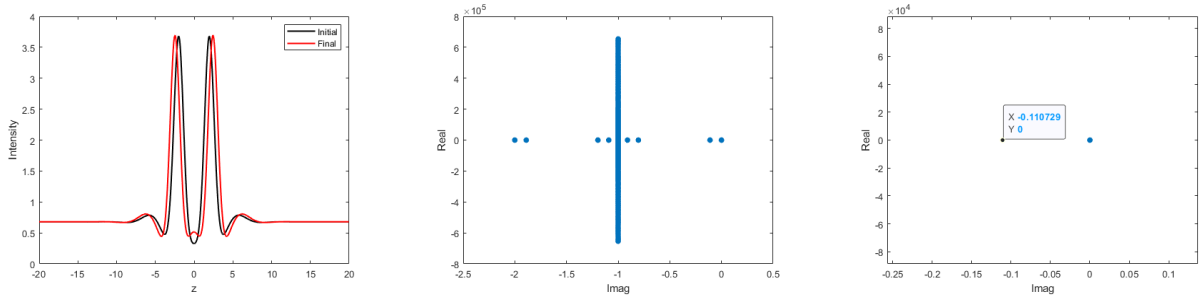

(a) Initial and final time (b) Spectrum of linearization (c) Eigenvalue closest to zero

Figure 4.15: Stable double pulse solution and its associated spectrum

Figure 4.16 shows all double pulse solutions found for these parameter values. The five d_i each correspond to the five figures. The initial condition is shown in black and final solution is shown in red.

In summary, we found a discrete set of double pulse solutions, both stable and unstable, that exist for a given set of parameters. The change in the separation distance of the pulses between the double pulse solution states can be characterized by the interaction of the pulses via their tails. As the pulses get further apart, the spectral eigenvalue closest to zero, s_0, decreases in magnitude each time as shown in table 4.1. When the pulses are far enough apart, $s_0 \to 0$ demonstrating that after a certain distance apart, the pulses don't have any interaction in their tails and can thus be regarded as two single pulses existing in the same domain. These results are extended in chapter 5 when the domain length is varied.

4.3. Phase and Chirp

In optics, phase refers to a property of light waves that describes the position of a point in its cycle relative to a reference point [6]. Phase plays a crucial role in many optical phenomena, including interference, diffraction, and polarization. In applications such as optical imaging, communication systems, or frequency metrology, controlling and manipulating the phase of light waves is essential for achieving desired outcomes, such as enhancing resolution or encoding information.

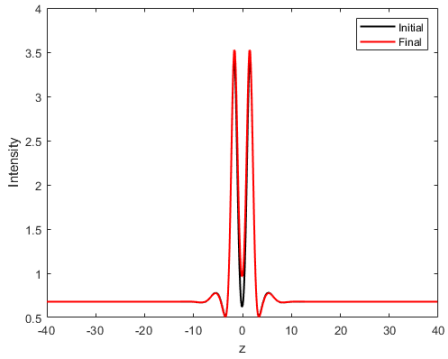

(a) Unstable corresponding to $d_i \approx 3.1$

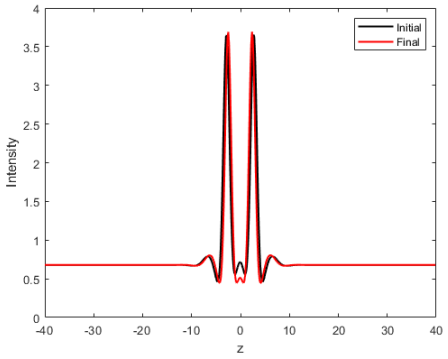

(b) Stable corresponding to $d_i \approx 4.8$

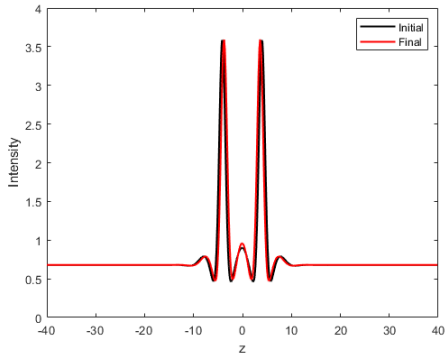

(c) Unstable corresponding to $d_i \approx 7.3$

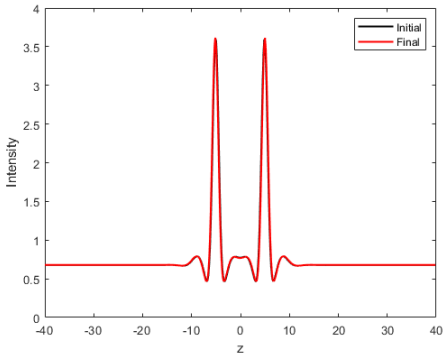

(d) Stable corresponding to $d_i \approx 10.1$

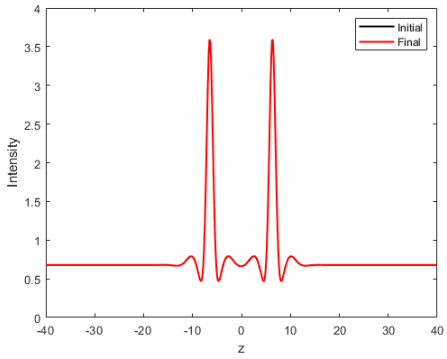

(e) Unstable corresponding to $d_i \approx 12.8$

Figure 4.16: Double pulse solutions found

Chirp (spatial/temporal) refers to a phenomenon where the derivative of the phase of the electromagnetic wave of a light wave varies with space or time. This variation can be linear or nonlinear and can occur in both special temporal and spectral domains [37] and has applications in the degenerate of ultrashort pulse durations. For example, in ultrashort pulse

lasers, the pulse duration can be stretched or compressed due to temporal chirp. In other words the stretching or compressing of the temporal chirp affects its temporal profile [19].

Spectral chirp, on the other hand, refers to changes in the frequency or phase of a light wave across its spectrum. This can occur, for instance, when light passes through a dispersive medium, such as a prism or a diffraction grating, where different frequencies propagate at different speeds, leading to a spreading or compression of the spectrum [39]. Spectral chirp is also crucial in phenomena like frequency modulation and dispersion compensation in optical communication systems. Chirp is a vital consideration in various optical systems and applications because it can affect the behavior of light waves and their interactions with matter.

The field envelope, E, of the quartic LLE (equation 1.4), can be expressed in amplitude-phase form:

$$E = |E|e^{i\varphi}$$

where φ is the phase. The instantaneous frequency, that is the derivative of the phase with respect to z (in LLE, z is time-like), if dependent on z, then the pulse is said to have a chirp. This is due to the effect of the quadratic dispersion and nonlinearities (SPM arising from the Kerr effect). Chirp occurs at high energies where you have high nonlinear effects and if these effects are not there, then you would not have a chirp.

The chirp is only relevant where there is a pulse, i.e. not in the background state. For a single pulse, the resulting phase is shown in Figure 4.17. The evolution of the phase is shown on the left and the final resulting phase is shown on the right. The phase can hence be expressed as an approximation inside the pulse

$$\varphi \approx \varphi_s + \alpha(z - z_0)(z - z_1) \tag{4.25}$$

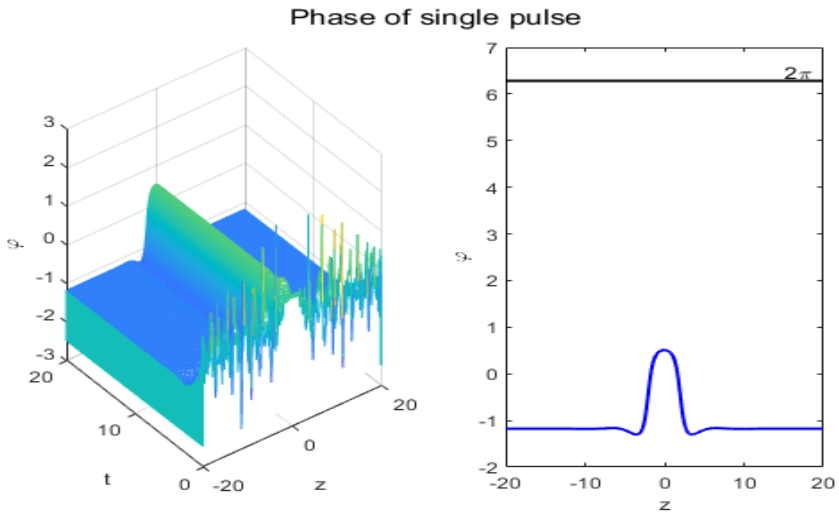

Figure 4.17: Resulting phase of a single pulse solution. The background constant phase corresponds to that of the CW solutions on the bottom part of the S-curve.

for a single pulse where φ_s is the constant background state corresponding to the CW solutions, E_s, that is if $E_s = |E_s|e^{i\varphi_s}$, then

$$\varphi_s = -i\ln(E_s/|E_s|).$$

The numbers z_0 and z_1 correspond to the points where the phase goes from being constant to something that is approximately quadratic. We point out from simulation, the phase takes an interesting profile for multi-pulse solutions and dark pulses (shown in figures 4.18 and 4.19) but only discuss the single pulse as the other are formulated in a similar manner.

In conclusion, the numerical studies carried out in this chapter provide insightful observations into the emergence of coherent structures. However more detailed statistical analysis is needed for initial conditions involving noise. Through our numerical explorations, we were able to see some unique dynamics of multi-pulses with varying pulse separation distances which we further explored for double pulse solutions with a large domain length emulating the problem being posed in an infinite line. These studies will further be explored in chap-

ter 6. We also investigated chirp for a variety of multi-pulse solutions which is a crucial consideration in optics to further study the behavior of light in a cavity.

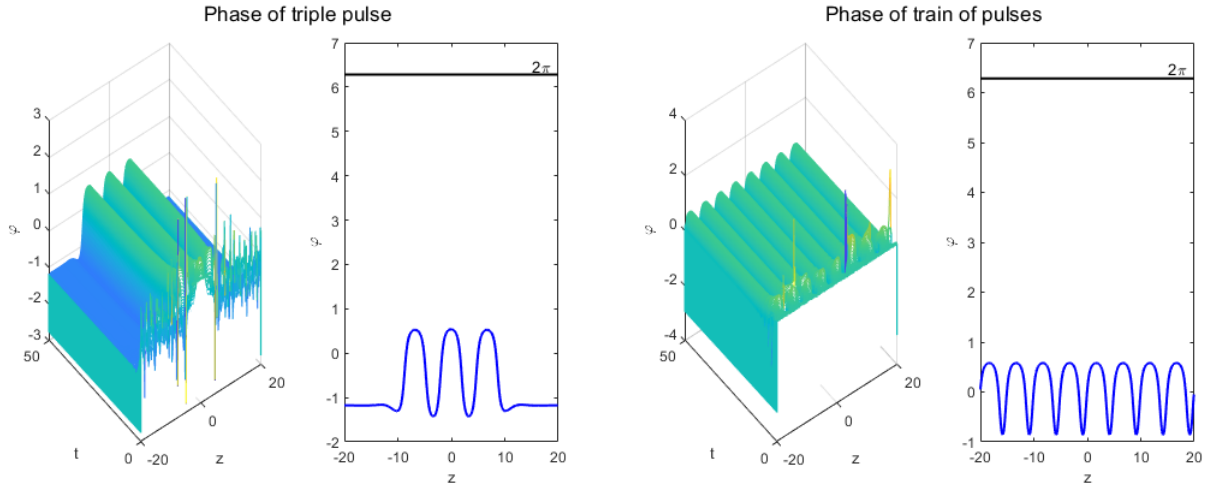

Figure 4.18: (left) Resulting phase of a triple pulse solution. Like in the single pulse case, the background phase corresponds to that of the CW solutions on the bottom part of the S-curve. (right) Resulting phase of a train of pulses, which is a periodic function.

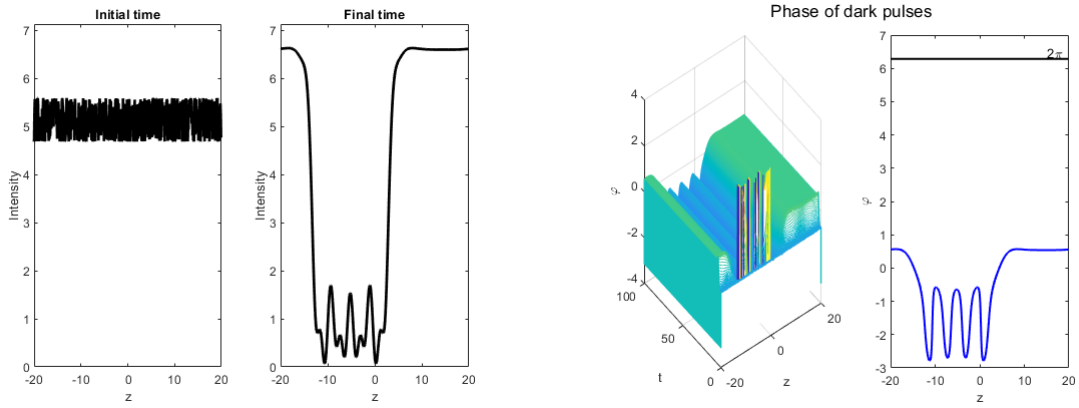

Figure 4.19: Left two pictures show the initial condition and final solution given $\beta_4 > 0$ leading to a dark pulse. The right two pictures show the resulting phase. Here, the background constant phase corresponds to the CW solutions on the top part of the S-curve.

Chapter 5

Stability and Dynamics of Various Pulse-Like Solutions of the Quartic LLE

This chapter discusses different stability properties and dynamics of various pulse-like solutions of the quartic LLE. The stability of multi-pulse solutions can be studied by looking at the spectrum of linearization of the underlying PDE about the solutions [29]. For the spectrally unstable double pulse solutions, the behavior in time of the quartic LLE, lead to interesting dynamics of the pulse separation distance which is investigated in section 5.2.

From a dynamical systems perspective, the CW solutions on the lower part of the S-curve are stable equilibrium points. The pulses have four-dimensional stable and unstable manifolds, given by the spatial eigenvalues of equation (3.3), which allows the possibility of the formation of a homoclinic orbit. In fact, this can be seen in figure 5.1 for a single pulse solution. The final steady state solution is denoted $E(T, z)$ where T is the final time. The plot on the left shows the final single pulse steady state solution and the right plot shows the projection of the real part of $E(T, z)$ and the real part of the first derivative $\frac{\partial}{\partial z}E(T, z)$. The background state is the CW solution corresponding to the lower part of the S-curve. The trajectory is ejected from the CW state to form the single bright pulse and then returns to the CW state to form a homoclinic orbit. This is similar to what happens in the case of only second-order dispersion in the LLE. Further techniques were investigated for this case in [31] for the LLE with quadratic dispersion.

5.1. Numerical Solutions and Decay Rate

In section 4.2, the spectral eigenvalues, defined as the eigenvalues of the matrix in equation (4.24), quantify the stability of solutions to the stationary quartic LLE. Recall, the

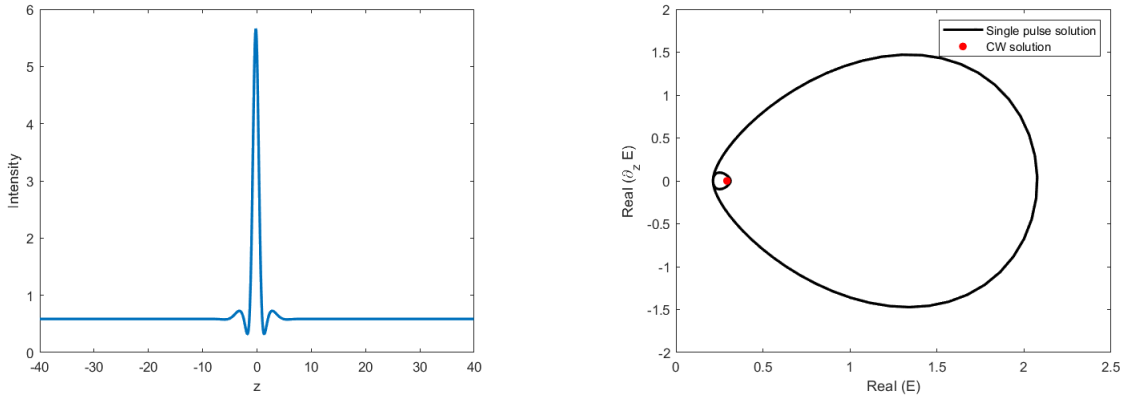

Figure 5.1: Single pulse solution and the corresponding phase plane trajectory

spectral eigenvalues are the result of the eigenvalues of the Jacobian from the spectrum of linearization of the solution. These eigenvalues can provide insight into how the solution responds to different frequencies of perturbations or disturbances [35].

When applying numerical methods to solve PDEs, it is crucial to ensure that the time step used in the simulation is small enough to capture the dynamics of the system accurately without causing numerical instability. This often involves analyzing the spectrum of the discretized system and choosing appropriate time step sizes based on the eigenvalues. The behavior of the eigenvalues influences the convergence rate of the numerical solution towards the steady state. By looking at the l^2 norm of the solution over time compared to the steady state solution, we can see if this solution is stable and also look at the decay rate.

Numerical investigations are done for multi-pulse structures consisting of three and five pulses. For the 3-pulse solution (shown in figure 5.2), the evolution plot is shown in the top left and the initial condition and final steady state solution is shown in the top right. Starting from localized noise, as described in equation (4.17), we obtain a multi-pulse solution consisting of three pulses. The bottom left figure shows the l^2 norm of the time to reach steady state. The bottom right figure is the spectrum of linearization of the final time steady state solution. The eigenvalue closest to zero is negative and has the value $s_0 = -0.0599$. The log of the l^2 norm, which is shown in the bottom left figure, is approximately linear and

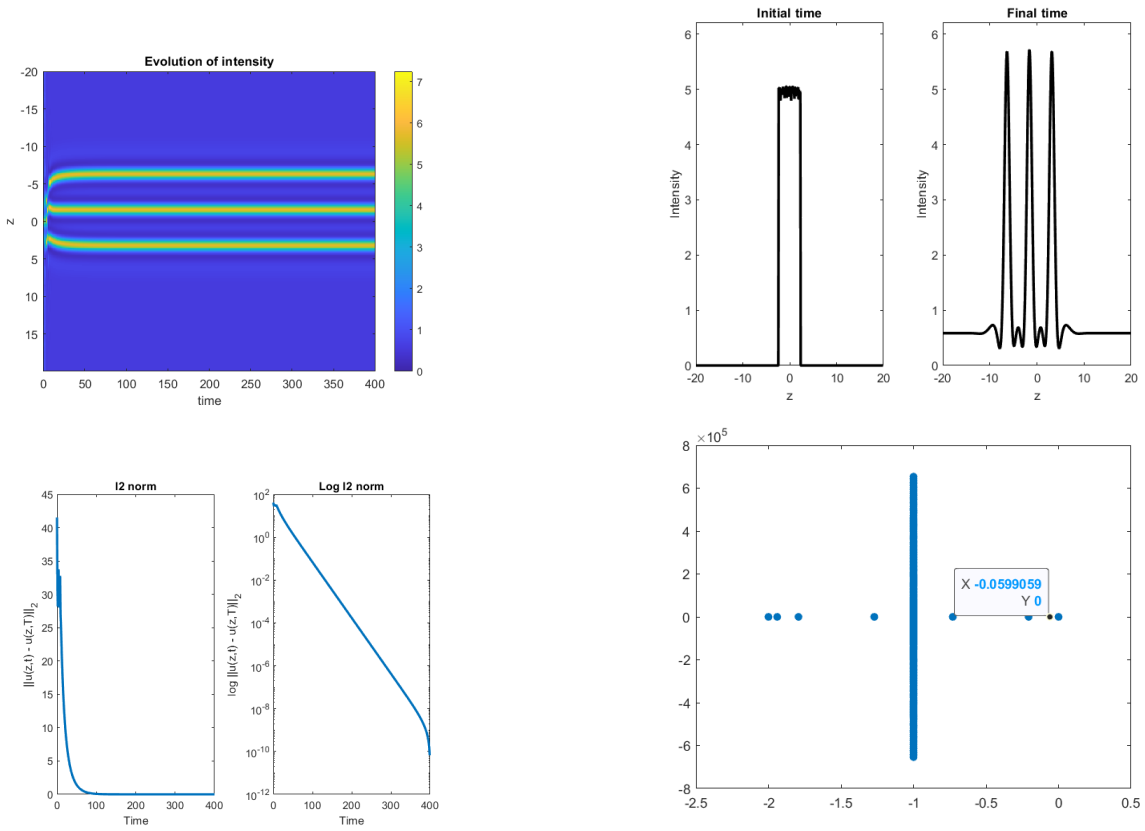

Figure 5.2: 3-pulse solution

when this line is approximated results in a slope of -0.0612. This value is approximately equivalent to the spectral eigenvalue closest to zero exhibiting to us that indeed the spectral eigenvalues relay information about the rate of decay of coherent structures for the quartic LLE.

Similarly for the coherent structure with five pulses shown in figure 5.3, the spectral eigenvalue closest to zero is $s_0 = -0.0213$. When using a linear fit of the log of the l^2 norm shown in the bottom left figure, this results in a slope of -0.0221 for the line. The values here are slightly smaller than the three-pulse case, hence why the solution takes longer to reach steady state. This direct relationship between the total time to reach steady state and the number of pulses in the final solution, indeed influence the magnitude of the spectral eigenvalue closest to zero. As the number of pulses increases in the final steady state solution, the number of orbits around the CW solution increases, thus taking it longer to return to

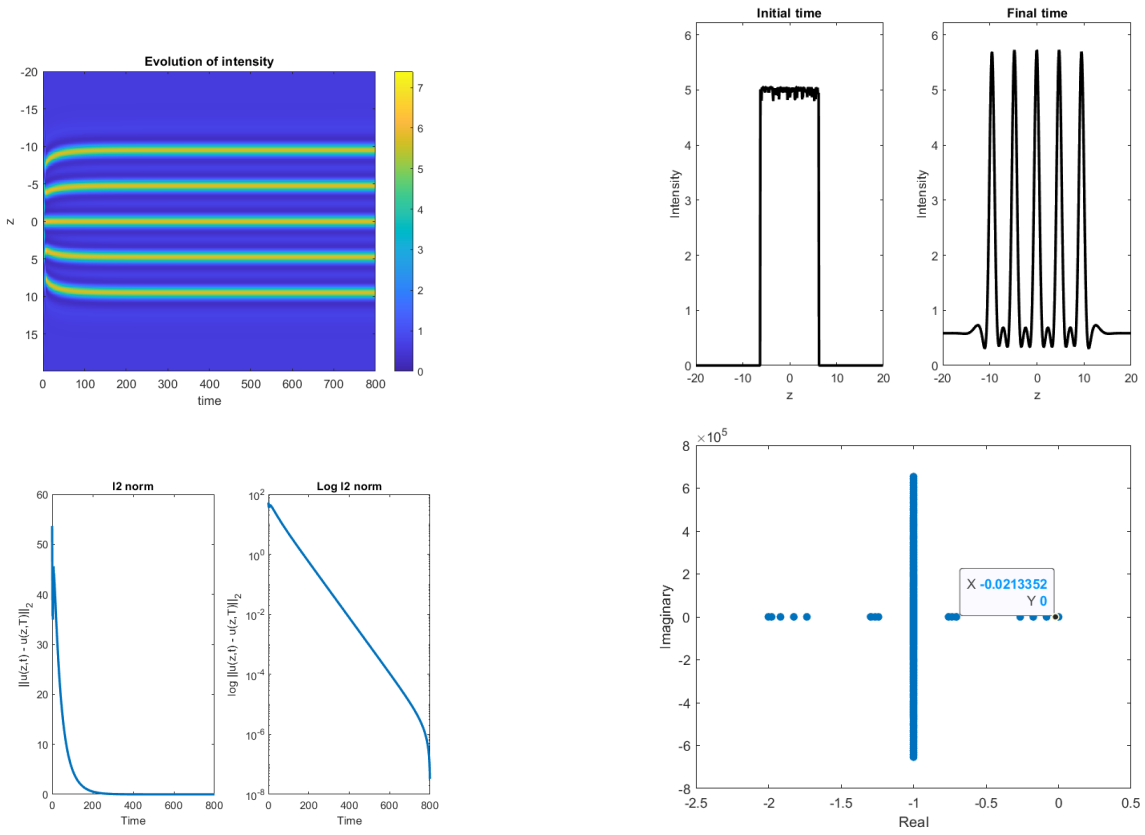

Figure 5.3: 5-pulse solution

the stable background state. Therefore, single pulse solutions take the fastest to converge and a train of pulses would take the longest to converge to steady state.

5.2. Double Pulse Stability

A discrete set of double pulse solutions were found in section 4.2, both linearly stable and unstable. The goal of this section is to observe the behavior of an unstable double pulse solution in time. By taking the double pulse, $E_d(z)$, we perturb it and use that as the initial condition for the quartic LLE, that is

$$E(0, z) = E_d(z) + \tilde{E}_d$$

where $\tilde{E}_d$ is the perturbation. Figures 5.4 and 5.5 show the two different scenarios that can happen. Given that for each unstable double pulse solution there are two "nearby" stable solutions, one with a smaller and one with larger separation distance between pulses, then one can expect the unstable solution will go to either one of those depending on the noise of the perturbation. The perturbed double pulse effectively acts as a one-dimensional dynamical system where the distance between the pulses near $z = 0$ is the dynamical variable. The stable and unstable double pulse solutions are thus acting as alternating attractors and repellers.

Summarizing, in this chapter we presented the stability and dynamics of various pulse-like solutions of the quartic LLE. We find that the decay rate of numerical solutions is approximately equivalent to that of the spectral eigenvalue closest to zero of the spectrum of linearization. This provides us with a tool to numerically estimate the time to reach steady state, namely it is identifying these eigenvalues and calculating its magnitude. Our results show that the time for coherent structures with multiple pulses to reach steady state increases with the number of pulses. Finally, the temporal dynamics of double pulse solutions shows that the spectrally unstable double pulse solutions act as repellers, and for the stable case, they act as attractors. This allows defining a one-dimensional dynamics for double pulse solutions with the inter-pulse separation distance being the dynamical variable.

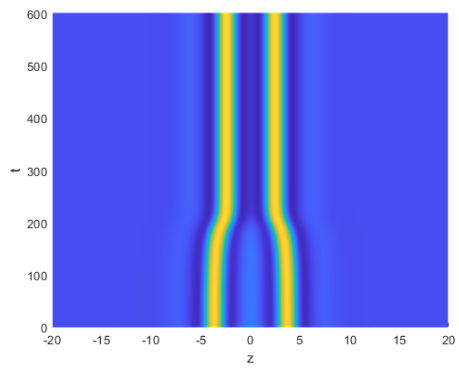

(a) Evolution of a double pulse solution starting from a perturbed unstable pulse. The figure shows a top down view of pulse separation distance. Here, the two pulse come closer together.

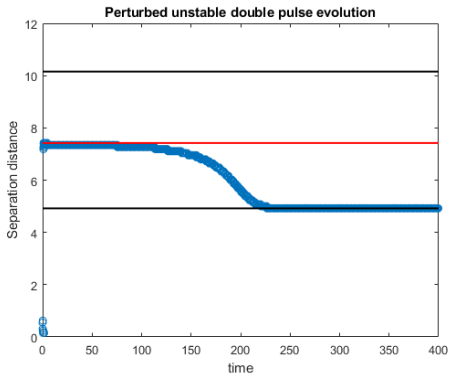

(b) Graph of the separation distance between the two pulses and time. Black lines are the stable separation distance and the red line is the unstable separation distance.

Figure 5.4: Separation distance going to smaller state.

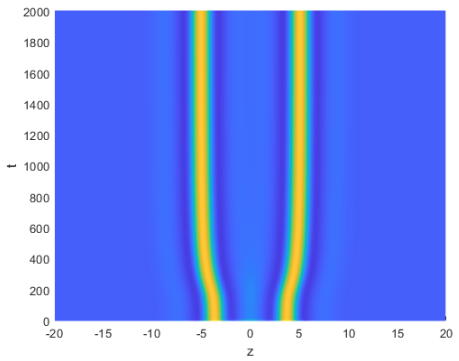

(a) Evolution of a double pulse solution starting from a perturbed unstable pulse. The figure shows a top down view of pulse separation distance. Here, the two pulse come closer together.

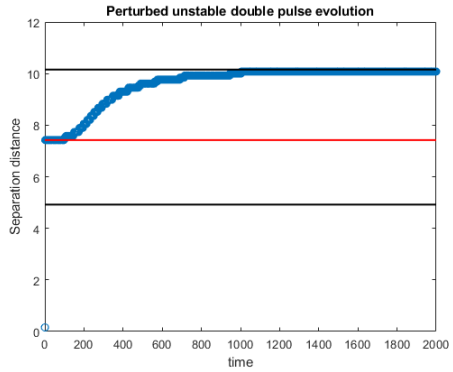

(b) Graph of the separation distance between the two pulses and time. Black lines are the stable separation distance and the red line is the unstable separation distance.

Figure 5.5: Separation distance going to larger state.

Chapter 6

Exploration of Multi-Pulses in a Ring

This chapter explores the interaction of multi-pulse solutions in a ring. The interaction of pure quartic solitons has been theoretically studied in the NLSE by means of the interaction potential of the PQSs based on the Hamiltonian of the system ([42] [11]). However, the dynamics of multi-pulse interactions have not been studied for the quartic LLE since, in particular, the approaches involving the Hamiltonian of the system do not apply since the LLE is non-conservative. These studies might be of interest for applications in long-distance optical communication systems and microresonators.

We still consider the quartic LLE on the interval $z \in [-L, L]$ where L is the domain length. In chapters 4 and 5, this parameter is taken to be either $L = 20$ or $L = 40$, which effectively represents the infinite line. Hence, we now consider a shorter domain length of $L \in [4, 20]$ to study the interaction of pulses in a circle. We still enforce the periodic boundary conditions $E(t, -L) = E(t, L)$ where $z \in [-L, L]$. The initial condition is the background state (E_s) summed with a pulse-like shape, that is

$$E(0, z) = E_s + \sum_{n=1}^{Q} sech\left(\frac{z - z_n}{\gamma}\right) \tag{6.1}$$

where Q is the number of pulses, z_n is the location of the center of the pulse, and γ is the pulse width. Figure 6.1 shows the evolution of the pulse separation distance for two to seven pulses for varying domain lengths. Since there is now interaction between neighbor pulses ahead and behind each one, one expects the competing repelling and attracting forces to equilibrate leading to an equidistant multi-pulse configuration. That is, they are separated by a distance of 2L/Q.

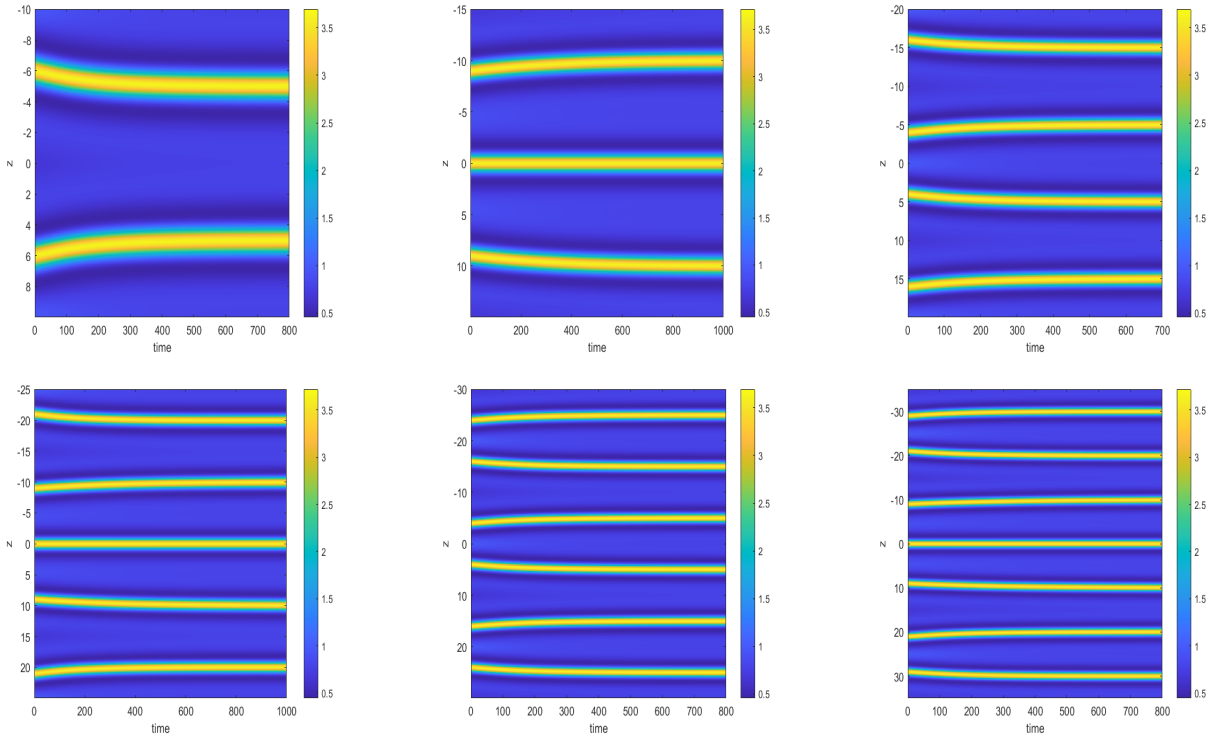

Figure 6.1: Evolution of pulse separation distance for two to seven pulses.

Figure 6.2 shows the number of pulses versus the total time it took for the pulses to reach steady state. One thing to note with constructing the pulses in this way is that the inherent symmetry along z=0 effectively makes the order of magnitude of the time to steady state much lower than expected as shown. Next we want to consider what will happen when we randomize the placement of the pulses in the initial condition to see the evolution and differences in time to steady state when this is done. We also want to see the differences between the quadratric dispersion case and the quartic dispersion case.

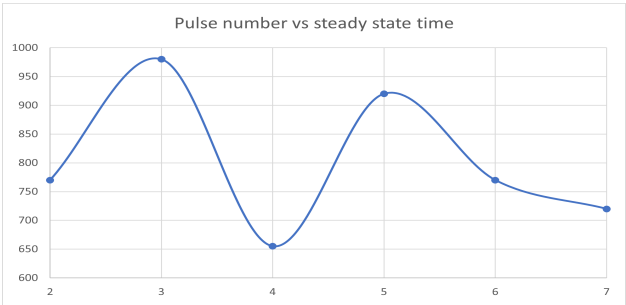

Figure 6.2: The number of pulses vs the time it took to reach steady state

For these simulations, L=7.5, N=1024, $\theta = 2.2$, P=1.5, and the dispersion parameter is specified in the figure. We consider the two cases where there is pure fourth order dispersion, $\beta_2 = 0$ and $\beta_4 = -1/4$ and the second case of only second order dispersion, that is $\beta_2 = 1$ and $\beta_4 = 0$.

When the placement of the pulse centers is random, the stable steady state achieved may not always be equidistant. Figure 6.3 illustrates that the dispersion parameter affects the stability of the equidistant solution. Figure 6.4 demonstrates that dominant fourth-order dispersion results in an increased number of pulses in the final steady-state solution compared to dominant second-order dispersion, albeit with a weaker intensity exchange in the former. However, in this scenario, both the equidistant two-pulse and three-pulse solutions remain stable. Figure 6.5 illustrates that while the number of pulses remains consistent with the initial condition shown at the start, the stable state varies across different dispersion parameter cases. Figure 6.6 presents another initial condition similar to that of figure 6.5, albeit with different centers for the three initial pulses. This leads to behavior similar to what we observe in figure 6.4. This numerical experimentation could indicate two things:

- The dominant order of dispersion plays a role in the stability of equidistant pulse solutions
- Stable multi-pulse solutions might be more attainable with dominant higher-order dispersion

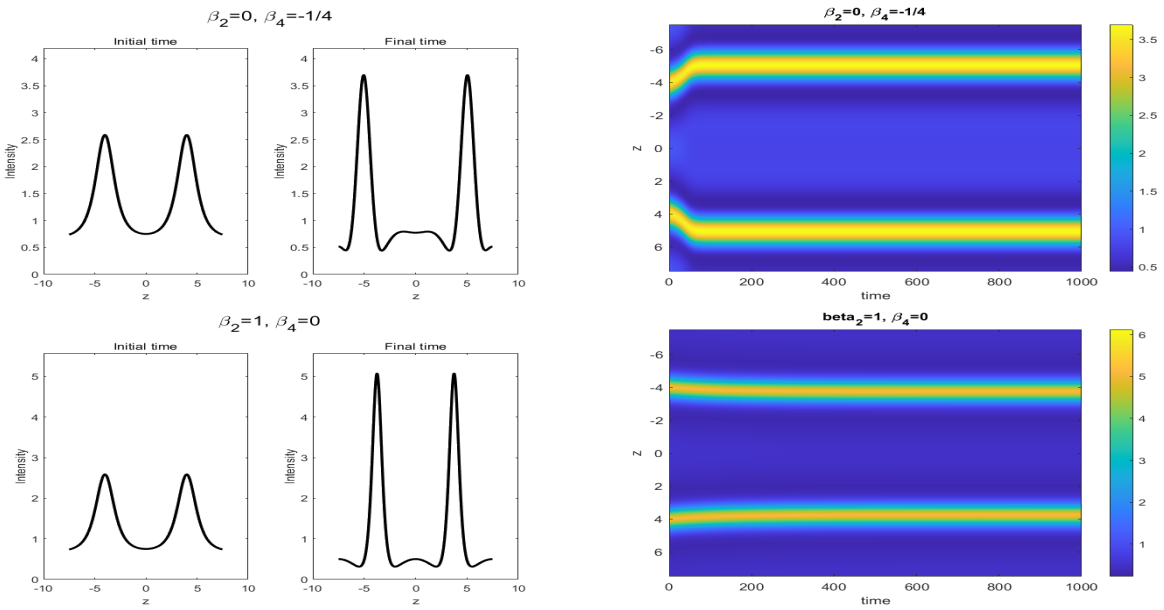

Figure 6.3: Top figures: Only fourth order dispersion; Bottom figures: Only second order dispersion. For the fourth order dispersion case, the pulses go to a stable double pulse solution state but they are not equidistance from each other. For the second order dispersion case, the pulses are equidistance from each other.

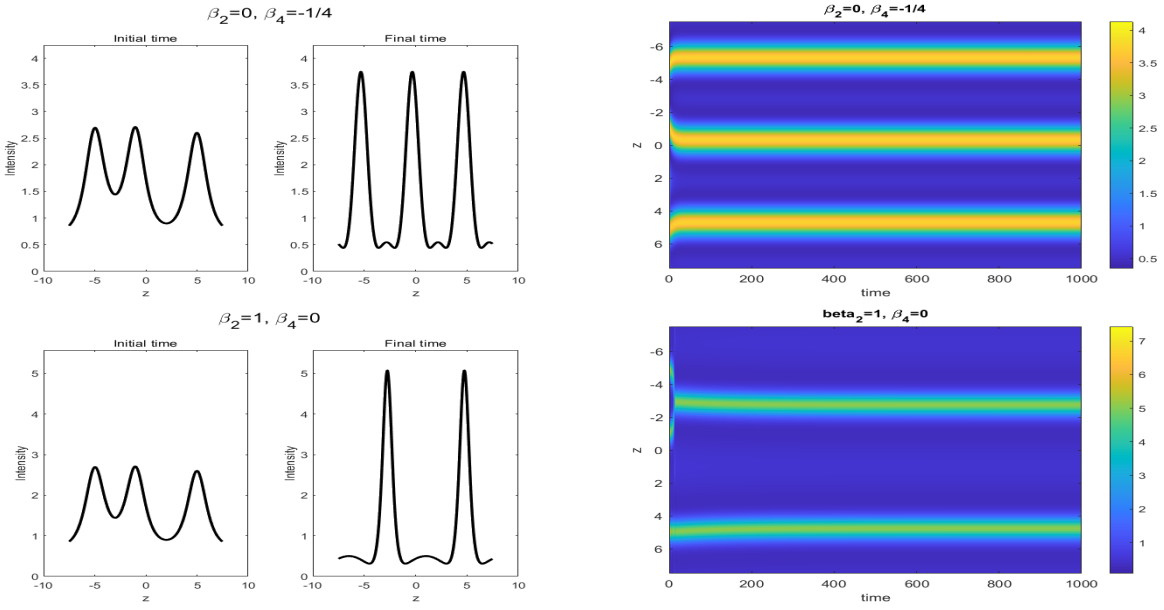

Figure 6.4: Top figures: Only fourth order dispersion; Bottom figures: Only second order dispersion. For the fourth order dispersion case, the steady state solution emits three pulses with each of those peaks separating in the initial condition. For the second order dispersion case, two of the pulses that were close together in the initial condition combine and the final steady state solution emits two pulses.

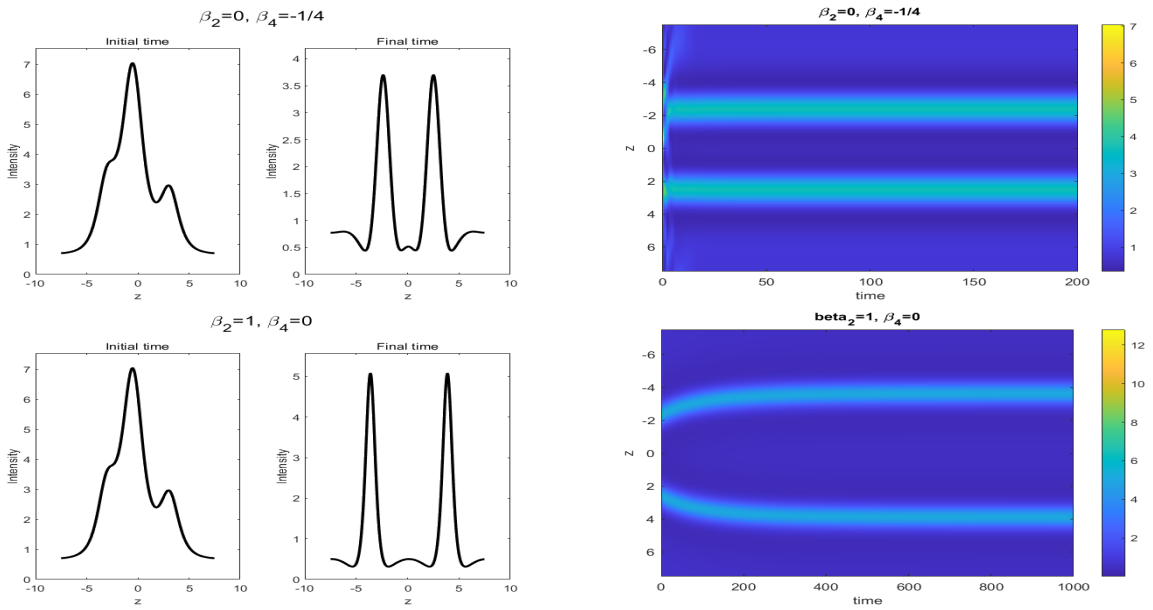

Figure 6.5: Top figures: Only fourth order dispersion; Bottom figures: Only second order dispersion. For the fourth order dispersion case, we get a stable double pulse solution and for the second order dispersion case, we get the stable equidistant double pulse solution.

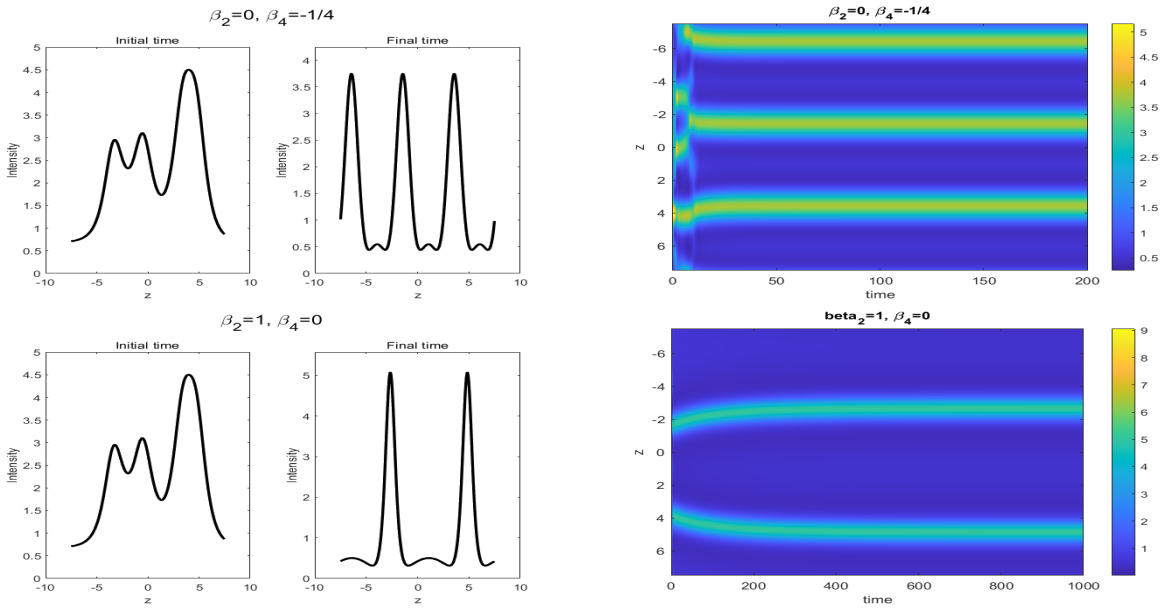

Figure 6.6: Top figures: Only fourth order dispersion; Bottom figures: Only second order dispersion. For the fourth order dispersion case, the steady state shows three pulses. For the second order dispersion case, we get two pulses.

To rigorously investigate these observations, we will initially concentrate on the scenario of double pulse solutions within a ring. Consider the following:

$$\begin{aligned} \frac{\partial E}{\partial t} &= -(1+i\theta)E + i|E|^2E - i\beta_2\frac{\partial^2 E}{\partial z^2} + i\beta_4\frac{\partial^4 E}{\partial z^4} + P \\ E(t,-L) &= E(t,L) \\ E(0,z) &= E_d(0,z;k) \end{aligned}$$

for $z \in [-L, L], t \in [0, T]$. That is, the generalized Lugiato-Lefever equation with second and fourth order dispersion for periodic boundary conditions and a two-pulse like initial condition (given in equation (4.19)). The goal is to find the stability of all two pulse solutions for a varying domain parameter L where there is different dominant orders of dispersion. Consider the two cases:

i Case 1: Dominant fourth order dispersion where $\beta_4 = -1/4$ and $\beta_2 = 0$

ii Case 2: Dominant second order dispersion where $\beta_4 = 0$ and $\beta_2 = 1$

Now, we want to define the parameter L such that $L = 2X_0 + 2X_1$ where X_0 is the distance from $z = 0$ to the peak of the pulse and X_1 is the distance from the peak of the pulse to $z = L$ (shown in figure 6.7). We saw in section 4.2 that there is a discrete family of double pulse solutions for L=40 until eventually the two pulses are far enough apart and they don't have any interaction so they can be regarded as two single pulses in the same line. The hypothesis is that this result could be extended for any domain length L.

Let us first investigate the role dispersion plays on the stability of the equidistant double pulse solutions for varying domain length L, that is when $X_0 = X_1$. As in section 4.2, the spectral stability is found by looking at the spectrum of linearization of the double pulse solution. The eigenvalues are denoted s_i where $i \in \mathrm{Z} \cap [0, N-1]$ and we define the eigenvalue closest to zero s_0. Most of the eigenvalues are negative except the one at zero due to the

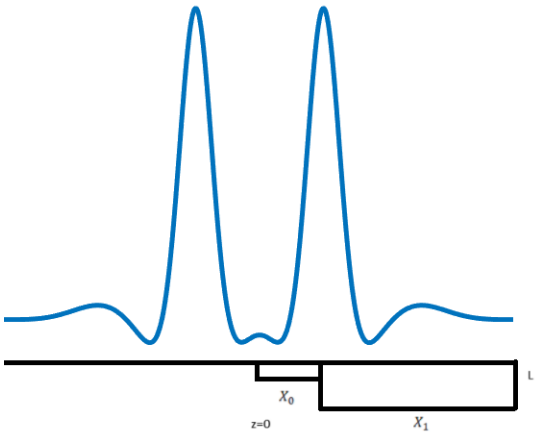

Figure 6.7: Setup of initial condition with two pulses for varying L

translation invariance property of the LLE and potentially s_0. If $s_0 < 0$, then the double pulse solution is stable and if $s_0 > 0$, then it is unstable.

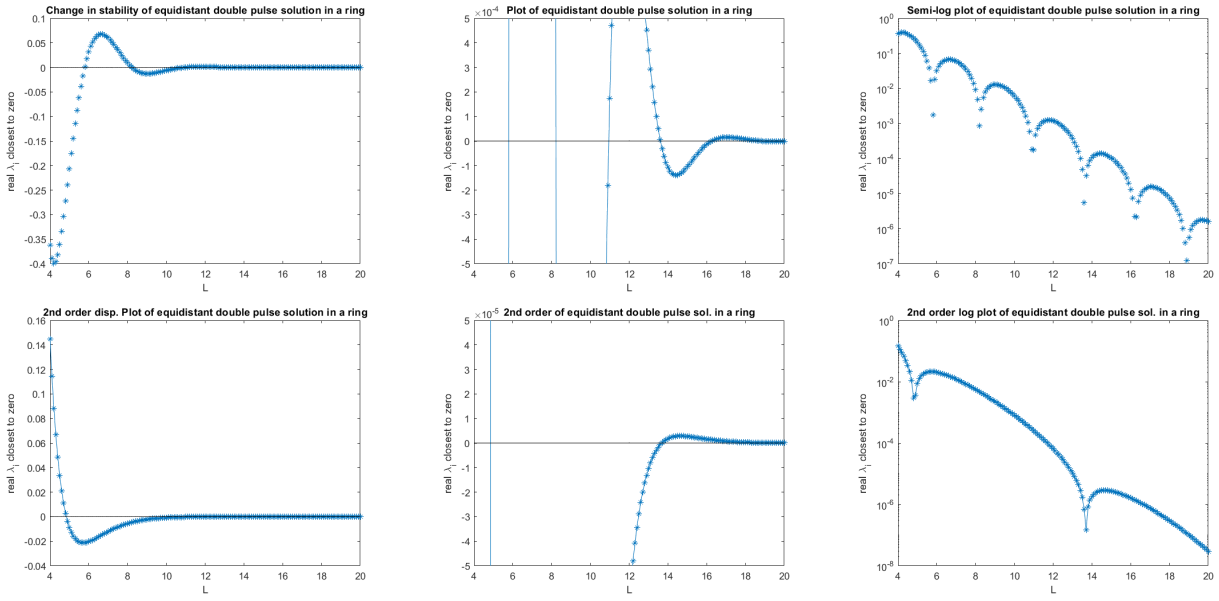

Figure 6.8: Change in stability of equidistant double pulse solution. First row: Case 1 of fourth order dispersion; Second row: Case 2 of second order dispersion

Figure 6.8 shows the change in stability of the equidistant double pulse solutions defined by s_0 as a function of the length of the ring L. The first column is the plot from $L \in [4, 20]$ showing the differences between having dominant second or fourth order dispersion. The second column is a close-up of the x-axis to further see the frequency of the switching in

stability. The third column is a log plot of the first column. This shows us that there is a more frequent shift in stability of the double pulse solution for the fourth order dispersion case and thus leading to much more interesting dynamics.

Focusing on the fourth-order dispersion case and now seeing what happens when $X_0 \neq X_1$, we want to see the stability of the family of double pulse solutions we get for different values of L. Figure 6.9 shows the resulting bifurcation plot of the stability of the double pulse solutions. The blue dots indicate a stable solution and a red dot indicates an unstable solution. The left plot is a three-dimensional plot of X_0, the distance from $z = 0$ to the peak of the pulse, X_1, the distance from the peak of the pulse to the end of the domain, and the domain length L. The right plot shows a two-dimensional projection comparing the domain length and the pulse separation distance. If you take a vertical line of the right plot, for example at L=12, this would tell you there are four double pulse solutions switching in stability each time as the distance between the pulses increases.

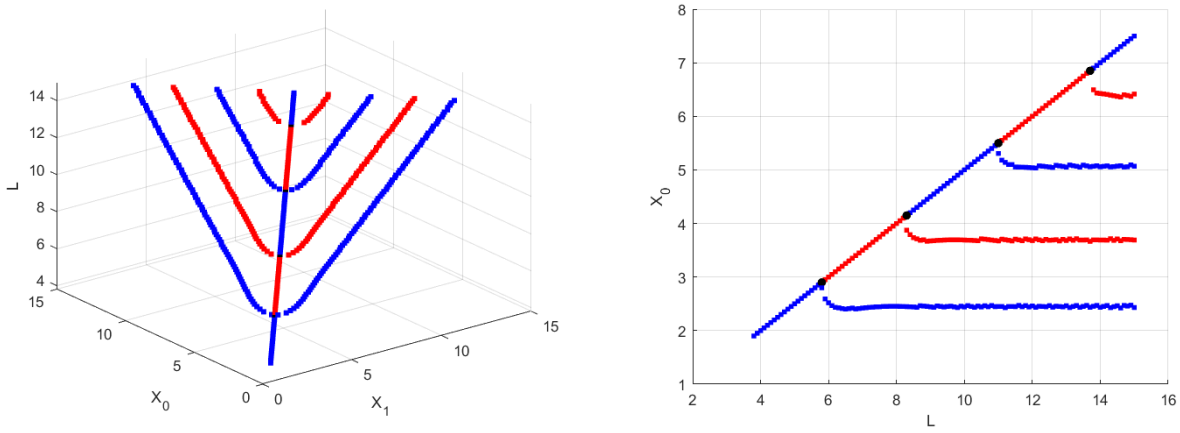

Figure 6.9: Bifurcation plots of stability of double pulse solutions

Briefly, we can also investigate the stability of three-pulse solutions. For three-pulses, there are two spectral eigenvalues to keep track of that are moving through zero. If the pulses are equidistant from each other, this eigenvalue is the same or equivalently, s_0 has a multiplicity of two. Figure 6.10 shows the change in stability of the equidistant three-pulse

solution for the fourth-order dispersion case (left), second-order dispersion case (middle), and a specific example of a non-equidistant stable triple pulse solution found.

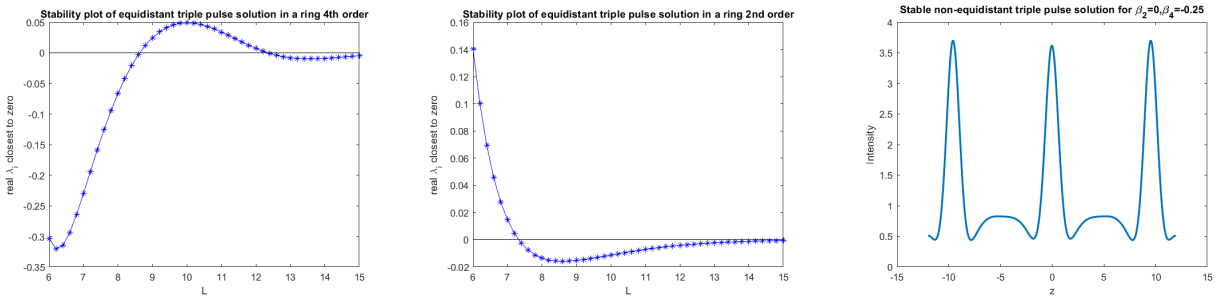

Figure 6.10: Three-pulse stability in a ring

Further investigation could be done in the three-pulse stability in a ring but based on preliminary numerical experiments, there does appear to exist stable non-equidistant multi-pulse solutions. These states, in a broader sense to all multi-pulse solutions, exist and are stable. For the three-pulse case, it is a product of two stable double pulse solutions. Therefore, for multi-pulse solutions, there could exist a stable non-equidistant state that is simply the sum of the stable non-equidistant double pulse states. As the the number of pulses considered in a ring increases, so does the number of spectral eigenvalues moving through the origin. For example, for a three-pulse solution, there are two eigenvalues passing through zero and switching stability. Generally, an n-pulse solution has n-1 spectral eigenvalues potentially switching stability thus increasing the complexity of finding stable multi-pulse solutions with varying pulse separation distances.

In various fields such as optics and signal processing, the power spectrum of intensity is often analyzed to understand the frequency composition of a signal or phenomena. Hence, the power spectrum of stable multi-pulse solutions in a ring is shown to see the spectral properties of the pulse dynamics (figure 6.11). Mathematically, the power spectrum is computed by taking the squared modulus of the fourier transform of the electric field E:

$$P(k) = |\mathcal{F}(E(T,z))|^2 \tag{6.2}$$

where k is the frequency and $\mathcal{F}$ is the fourier transform operator. These results match with those shown in experiments of PQS [12].

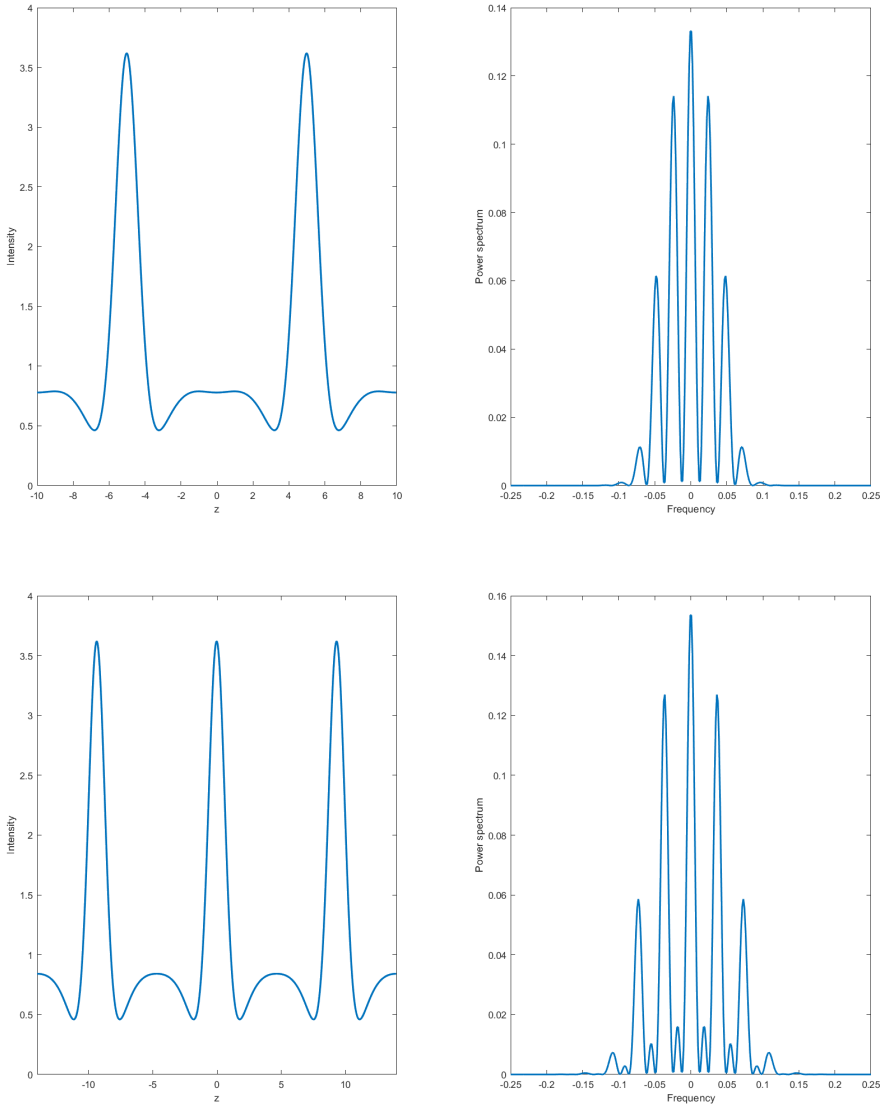

Figure 6.11: Stable equidistant multi-pulse solutions of the quartic LLE (left) and their corresponding power spectrum (right)

In conclusion, the interaction of multi-pulses in a ring lead to interesting dynamics that have applications in optical communications, spectroscopy, and more. Some novel dynamics for the quartic LLE are shown for a discrete family of double pulse solutions that exist for varying domain length and whose stability alternates as the inter-pulse separation distance

increases. These results could be used as a baseline to extend to the case of multi-pulses in a ring. Finally, the power spectrum of equidistant stable multi-pulses is shown as this has applications to frequency metrology.

Chapter 7

Summary and Conclusion

Solitons, or solitary waves that maintain their shape and structure while traversing through a medium, stand as remarkable phenomena with countless applications, particularly in the realm of optics. Their emergence is intricately tied to the balance between nonlinear and dispersive effects. This indeed lies our focus: exploring the world of higher-order dispersion, particularly the dominance of fourth-order dispersion, within nonlinear laser systems. Engineered solitons with higher-order dispersion hold promise for generating ultra-short, high-energy pulses, holding potential with far-reaching implications across diverse domains including frequency comb generation, telecommunications, and beyond. Leveraging the quartic Lugiato-Lefever Equation (LLE) serves as a mathematical model, offering a glimpse into the sophisticated dynamics of Pure Quartic Solitons (PQS) inside an optical cavity.

Initially, we describe the existence and stability of Continuous Wave (CW) solutions within the quartic LLE framework. These solutions serve as a baseline upon which further analyses are built. Delving deeper, we examine the spatial dynamics underpinning coherent structures, identifying key regions within the parameter space where these structures may manifest. We find this exhibits more intricate dynamics compared to their second-order dispersion counterparts indicating increased opportunities for the generation of coherent structures across the parameter space. It would be interesting to expand these studies for higher-order dispersion in the LLE, including sixth and eighth-order dispersion to examine the increased complexity of the spatial dynamics and the potential of the generation of pulses.

By doing numerical explorations, we provide investigations of coherent structures within the quartic LLE setting. Yet, amidst the observations of our numerical findings, the need for further statistical analysis looms large. There is a necessity to ascertain the robustness and validity of our numerical solutions. It would also be intriguing to quantify different ways to control the number of pulses generated from noise. This could lead to the investigation of other kinds of dynamics exhibited by the quartic LLE.

The interaction of solitary waves is an important consideration for many applications. Using the theory laid out by the spatial eigenvalues, we are able to uncover a discrete set of double pulse solutions under specific parameter regimes. This revelation sheds light on the complex interplay between pulses within the quartic LLE framework, offering glimpses into the structure of nonlinear wave interactions. This is further investigated in the focus of ring cavities. This yields novel insights into the dynamics of pulse interactions within the quartic LLE. It was demonstrated that a set of double pulse solutions for varying domain sizes gives rise to a pitchfork bifurcation of stable and unstable double pulse solutions whose dynamics are leveraged through pulse separation distances. These findings, show the intricate nature of the quartic LLE, revealing a complexity that is vastly different than its second-order dispersion counterpart.

Although not considered in this report, there has been some work in studying pure quartic solitons in other experimental settings. Indeed in [4], the Raman effect is considered with the effects of higher order dispersion. They report the numerical observation of PQS in Kerr microresonators and are investigated using a combined approach of numerics and analytics. As mentioned in the first section, for pulses with short pulse width, the energy of PQS are much higher than the conventional case of quadratic dispersion. In micro-cavities, the material stimulated Raman scattering is non-negligible due to these high-energy, ultrashort pulses. The investigation of Raman PQS is thus considered in [25]. In the presence of Raman, these homogeneous, stationary solutions are the same but the stability analysis is far more

complicated and could potentially require complicated analytical methods to provide more accurate results. In any case, the effects of higher-order dispersion or of Raman, all involve studying the evolution dynamics originating from the background state. However, the spatial dynamics and emergence of coherent structures when including the Raman term which could lead to more interesting dynamics.

In conclusion, the exploration of fourth-order dispersion within the framework of the Lugiato-Lefever Equation (LLE) has unveiled valuable insights of phenomena encompassing soliton generation, interaction, and dynamic behavior in nonlinear optical systems. Through theoretical analysis and numerical simulations, this research has illuminated the intricate balance between nonlinear effects and higher-order dispersion, shedding light on the emergence and stability of coherent structures of PQSs within an optical cavity. Moving forward, continued exploration into the interplay of higher-order dispersion and nonlinear effects promises to uncover further complexities and opportunities for advancing the field of nonlinear optics, paving the way for innovative technologies and applications in photonics.

BIBLIOGRAPHY

[1] Govind P. Agrawal. *Nonlinear Fiber Optics*. Academic Press, San Diego, CA, USA, 2001. 28

[2] N. Akhmediev and A. Ankiewicz. *Solitons: nonlinear pulses and beams*. Chapman & Hall/CRC, 2005. 2

[3] G.A. Askaryan. Cerenkov Radiation and Transition Radiation from Electromagnetic Waves. *Journal of Experimental and Theoretical Physics*, 15(5):943–6, 1962. 6

[4] Changjing Bao, Hossein Taheri, Lin Zhang, Andrey Matsko, Yan Yan, Peicheng Liao, Lute Maleki, and Alan E. Willner. High-order dispersion in kerr comb oscillators. 34(4):715–725. Publisher: Optica Publishing Group. 70

[5] Andrea Blanco-Redondo, C. Martijn de Sterke, J. E. Sipe, Thomas F. Krauss, Benjamin J. Eggleton, and Chad Husko. Pure-quartic solitons. 7(1):10427. Publisher: Nature Publishing Group. 3, 7

[6] Max Born and Emil Wolf. *Principles of Optics: Electromagnetic Theory of Propagation, Interference and Diffraction of Light*. Cambridge University Press, 7th edition, 1999. 47

[7] R. W. Boyd and D. J. Gauthier. *Nonlinear Optics*. Academic Press, 2008. 6, 7

[8] Wesley B. Cardoso, Luca Salasnich, and Boris A. Malomed. Localized solutions of lugiato-lefever equations with focused pump. 7(1):16876. Publisher: Nature Publishing Group. 10

[9] Ivan P. Christov, Margaret M. Murnane, Henry C. Kapteyn, Jianping Zhou, and Chung-Po Huang. Fourth-order dispersion-limited solitary pulses. *Opt. Lett.*, 19(18):1465–1467, Sep 1994. 3

[10] E. Cumberbatch. Self-focusing in Non-linear Optics. *IMA Journal of Applied Mathematics*, 6(3):250–262, 09 1970. 6

[11] Jiaxin Dai, Jiali Zeng, Wei Hu, and Daquan Lu. The bound states of pure-quartic solitons. 165:112867. 58

[12] C. Martijn de Sterke, Antoine F. J. Runge, Darren D. Hudson, and Andrea Blanco-Redondo. Pure-quartic solitons and their generalizations—theory and experiments. 6(9):091101. 5, 18, 67

[13] Ralf Deiterding, Roland Glowinski, Hilde Oliver, and Stephen Poole. A reliable split-step fourier method for the propagation equation of ultra-fast pulses in single-mode optical fibers. *Journal of Lightwave Technology*, 31(12):2008–2017, 2013. 28

[14] Peng Gao, Li-Zheng Lv, and Xin Li. Dark solitons and their bound states in a nonlinear fiber with second- and fourth-order dispersion, 2024. 39

[15] H. M. Gibbs. *Optical bistability: Controlling light with light*. 1985. 12

[16] H. M. Gibbs, S. L. McCall, and T. N. C. Venkatesan. Differential gain and bistability using a sodium-filled fabry-perot interferometer. *Phys. Rev. Lett.*, 36:1135–1138, May 1976. 12

[17] M.Y. Hamza and S. Tariq. Split step fourier method based pulse propagation model for nonlinear fiber optics. In *2007 International Conference on Electrical Engineering*, pages 1–5, 2007. 28

[18] A. Hasegawa and F. Tappert. Transmission of stationary nonlinear optical pulses in dispersive dielectric fibers. *Applied Physics Letters*, 23(3):142–144, 1973. 1

[19] Kyung-Han Hong, Jae Sung, Yong Lee, and Chang Nam. Temporal characterization of chirped femtosecond laser pulses. *Optics Communications*, 213:193–200, 12 2002. 49

[20] Anders Höök and Magnus Karlsson. Ultrashort solitons at the minimum-dispersion wavelength: effects of fourth-order dispersion. *Opt. Lett.*, 18(17):1388–1390, Sep 1993. 3

[21] Gerald W. Johnson and Michel D. Kruskal. *Solitons and Nonlinear Wave Equations*. Academic Press, 1973. 2

[22] D. J. Korteweg and G. de Vries. On the change of form of long waves advancing in a rectangular canal, and on a new type of long stationary waves. *Philosophical Magazine*, 39(240):422–443, 1895. 1

[23] P. Lallemand and N. Bloembergen. Self-focusing of laser beams and stimulated raman gain in liquids. *Phys. Rev. Lett.*, 15:1010–1012, Dec 1965. 6

[24] François Leo, Lendert Gelens, Philippe Emplit, Marc Haelterman, and Stéphane Coen. Dynamics of one-dimensional kerr cavity solitons. *Opt. Express*, 21(7):9180–9191, Apr 2013. 18

[25] Kewei Liu, Shunyu Yao, and Changxi Yang. Raman pure quartic solitons in kerr microresonators. 46(5):993–996. Publisher: Optica Publishing Group. 3, 70

[26] L. A. Lugiato and R. Lefever. Spatial dissipative structures in passive optical systems. 58(21):2209–2211. Publisher: American Physical Society. 8, 12, 13, 16

[27] Oliver Melchert and Ayhan Demircan. pyglle: A python toolkit for solving the generalized lugiato–lefever equation. *SoftwareX*, 15:100741, 2021. 32

[28] Alexander U. Nielsen, Yiqing Xu, Caleb Todd, Michel Ferré, Marcel G. Clerc, Stéphane Coen, Stuart G. Murdoch, and Miro Erkintalo. Nonlinear localization of dissipative modulation instability. *Phys. Rev. Lett.*, 127:123901, Sep 2021. 10

[29] Ross Parker and Alejandro Aceves. Multi-pulse solitary waves in a fourth-order nonlinear schrödinger equation. 422:132890. 32, 52

[30] P Parra-Rivas, D Gomila, P Colet, and L. Gelens. Interaction of solitons and the formation of bound states in the generalized lugiato-lefever equation. *Eur. Phys. J. D*, 71:198, 2017. 44

[31] P. Parra-Rivas, D. Gomila, L. Gelens, and E. Knobloch. Bifurcation structure of localized states in the lugiato-lefever equation with anomalous dispersion. 97(4):042204. Publisher: American Physical Society. 18, 23, 32, 52

[32] P. Parra-Rivas, D. Gomila, M. A. Matias, S. Coen, and L. Gelens. Dynamics of localized and patterned structures in the lugiato-lefever equation determine the stability and shape of optical frequency combs. 89(4):043813. 14, 18, 32

[33] Pedro Parra-Rivas, Sabrina Hetzel, Yaroslav V. Kartashov, Pedro Fernández de Córdoba, J. Alberto Conejero, Alejandro Aceves, and Carles Milián. Quartic kerr cavity combs: bright and dark solitons. 47(10):2438–2441. Publisher: Optica Publishing Group. 12, 18, 20, 32

[34] John S. Russell. Report on waves. *Report of the Fourteenth Meeting of the British Association for the Advancement of Science*, 1844. York. 1

[35] Björn Sandstede. Stability of multiple-pulse solutions. *Trans. Amer. Math. Soc.*, 350:429–472, 02 1998. 53

[36] A. J Scroggie, W. J Firth, G. S McDonald, M Tlidi, R Lefever, and L. A Lugiato. Pattern formation in a passive kerr cavity. 4(8):1323–1354. 12, 15, 16

[37] Anthony E Siegman. *Lasers*. University Science Books, 1986. 48

[38] R. H. Stolen and Chinlon Lin. Self-phase-modulation in silica optical fibers. *Phys. Rev. A*, 17:1448–1453, Apr 1978. 6

[39] Paul Tannouri and Israel Delgado. Spectral chirp measurement for dispersion characterization of optical fibers and components. *IEEE Photonics Technology Letters*, 24(15):1285–1287, 2012. 49

[40] Bastien Varlot, Stefan Wabnitz, Julien Fatome, Guy Millot, and Christophe Finot. Experimental generation of optical flaticon pulses. *Opt. Lett.*, 38(19):3899–3902, Oct 2013. 38

[41] V. E. Zakharov and A. B. Shabat. Exact theory of two-dimensional self-focusing and one-dimensional self-modulation of waves in nonlinear media. *Soviet Physics JETP*, 34(1):62–69, 1972. 2

[42] Jiali Zeng, Jiaxin Dai, Wei Hu, and Daquan Lu. Theory for the interaction of pure-quartic solitons. 129:107923. 58